https://doi.org/10.1093/plcell/koad121 THE PLANT CELL 2023: 35: 2952–2971

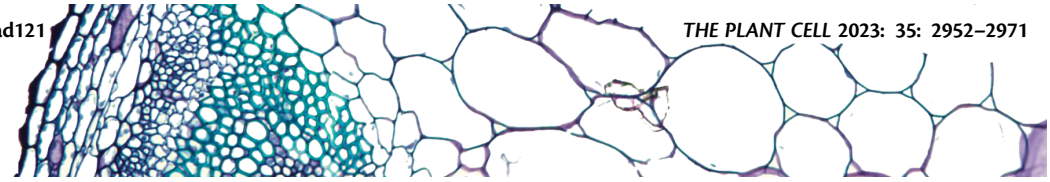

Research Article

The miR165/166–*PHABULOSA* module promotes thermotolerance by transcriptionally and posttranslationally regulating HSFA1

Jie Li [1], **Yiming Cao** [1], **Jiaxin Zhang** [1], **Cuijing Zhu** [1], **Guiliang Tang** [2] and **Jun Yan** [1,*]

1 School of Life Sciences, East China Normal University, Shanghai 200241, People's Republic of China
2 Department of Biological Sciences, Michigan Technological University, Houghton, MI 49931, USA

*Author for correspondence: jyan@bio.ecnu.edu.cn
The authors responsible for distribution of materials integral to the findings presented in this article in accordance with the policy described in the Instructions for Authors (https://academic.oup.com/plcell/) is: Jun Yan (jyan@bio.ecnu.edu.cn)

Abstract

Heat stress (HS) adversely affects plant growth and productivity. The Class A1 HS transcription factors (HSFA1s) act as master regulators in the plant response to HS. However, how HSFA1-mediated transcriptional reprogramming is modulated during HS remains to be elucidated. Here, we report that a module formed by the microRNAs miR165 and miR166 and their target transcript, *PHABULOSA* (*PHB*), regulates HSFA1 at the transcriptional and translational levels to control plant HS responses. HS-triggered induction of *MIR165/166* in *Arabidopsis thaliana* led to decreased expression of target genes including *PHB*. *MIR165/166* overexpression lines and mutations in miR165/166 target genes enhanced HS tolerance, whereas miR165/166 knockdown lines and plants expressing a miR165/166-resistant form of *PHB* were sensitive to HS. PHB directly repressed the transcription of *HSFA1*s and globally modulated the expression of HS-responsive genes. PHB and HSFA1s share a common target gene, *HSFA2*, which is essential for activation of plant responses to HS. PHB physically interacted with HSFA1s and exerted an antagonistic effect on HSFA1 transcriptional activity. PHB and HSFA1s co-regulated transcriptome reprogramming upon HS. Together, these findings indicate that heat-triggered regulation of the miR165/166–*PHB* module controls HSFA1-mediated transcriptional reprogramming and plays a critical role during HS in *Arabidopsis*.

Introduction

Plants are frequently challenged by extreme temperatures, which can adversely affect growth, development, distribution, and productivity. To acclimate to such stresses, plants have evolved strictly controlled regulatory mechanisms. When subjected to heat stress (HS), the expression of HS-responsive (*HSR*) genes is induced by HS transcription factors (HSFs). Plants contain more than 20 HSFs, which can be classified into 3 classes (A, B, and C) based on their oligomerization domains (Nover et al. 2001; Baniwal et al. 2004). In *Arabidopsis* (*Arabidopsis thaliana*), the 4 Class A1 HS transcription factors (HSFA1s), HSFA1a, HSFA1b, HSFA1d, and HSFA1e, act as master regulators of HS responses (Ohama et al. 2016).

With the exception of HSFB5, Class B HSFs contain the tetrapeptide motif LFGV and function as repressors in the regulation of *HSR* gene expression (Czarnecka-Verner et al. 2004; Ikeda and Ohme-Takagi 2009; Kumar et al. 2009; Ikeda et al. 2011). *HSFA2*, another *HSF* gene, serves as a direct target of HSFA1s and is crucial for the activation of *HSR* gene expression in plants (Charng et al. 2007). HSFs recognize and bind to heat shock elements (HSE: 5′-GAAnnTTC-3′) in the promoters of *HSR* genes to promote the accumulation of heat shock proteins (HSPs) (Busch et al. 2005). These HSPs are grouped into 5 classes according to their approximate molecular weight and include HSP100, HSP90, HSP70, HSP60, and small HSPs (sHSPs, 15–30 kD) (Vierling 1991; Trent 1996). HSPs function as molecular chaperones and maintain

Received February 14, 2023. Accepted April 09, 2023. Advance access publication May 3, 2023

cellular proteostasis by preventing protein aggregation and denaturation.

In addition to protein factors, increasing evidence shows that microRNAs (miRNAs) are vital regulators of HS responses. miRNAs are noncoding RNAs that are processed from primary transcripts into ~21-nucleotide-long molecules by the DICER-LIKE1 (DCL1)-associated processing complex and are essential for regulating plant growth and stress responses (Jones-Rhoades and Bartel 2004; Sunkar and Zhu 2004; Baker et al. 2005; Fujii et al. 2005; Lauter et al. 2005; Jones-Rhoades et al. 2006; Reyes and Chua 2007; Zhou et al. 2007; Khraiwesh et al. 2012; Rogers and Chen 2013). In *Arabidopsis*, miR398 strongly accumulates upon HS, while the transcript levels of its target genes such as *COPPER/ZINC SUPEROXIDE DISMUTASE 1* (*CSD1*), *CSD2*, and *COPPER CHAPERONE FOR CSD1 AND CSD2* (*CCS*) decrease (Guan et al. 2013). Single mutant plants lacking CSD1, CSD2, or CCS function are more tolerant to HS. By contrast, transgenic plants expressing forms of *CSD1*, *CSD2*, and *CCS* transcripts that are resistant to miR398-mediated cleavage are more vulnerable to HS than the wild type (WT) (Guan et al. 2013).

NAT398b/c are natural antisense transcripts of *MIR398b/c* genes and inhibit miR398 biogenesis, attenuating plant thermotolerance (Li et al. 2020). Additionally, heat-induced tocopherol (vitamin E) production promotes miR398 accumulation and improves heat tolerance (Fang et al. 2019). These results highlight the importance of miR398 abundance in plant thermotolerance. Other small RNAs, such as miR156, miR160, and *trans*-acting small interfering RNAs (ta-siRNAs), also play critical roles in the regulation of plant thermotolerance. miR156 regulates HS memory through SQUAMOSA-PROMOTER BINDING-LIKE (SPL) transcription factors (Stief et al. 2014). miR160 modulates the transcript levels of *AUXIN RESPONSE FACTOR* (*ARF*) genes to mediate heat tolerance (Lin et al. 2018). ta-siRNAs regulate their target genes *HEAT-INDUCED TAS1 TARGET 1* (*HTT1*) and *HTT2*, to modulate plant responses to HS (Li et al. 2014).

The highly conserved miRNAs miR165/166, which differ by a single nucleotide, play essential roles in different biological processes by regulating members of the Class *III HD-ZIP* transcription factor family including *PHABULOSA* (*PHB*), *PHAVOLUTA* (*PHV*), *REVOLUTA* (*REV*), *ATHB-8*, and *ATHB-15*. Despite their close relationship, *HD-ZIP III* members also have antagonistic functions. *HD-ZIP III* genes are needed for patterning of different organs, as shown in previous studies (Mcconnell et al. 2001; Otsuga et al. 2001; Prigge et al. 2005; Carlsbecker et al. 2010; Smith and Long 2010; Lucas et al. 2013). Furthermore, the interconnection between HD-ZIPIII proteins and core components of the auxin, cytokinin, and abscisic acid network has also been uncovered (Jia et al. 2015; Yan et al. 2016; Sessa et al. 2018). Additionally, miR165 and miR166 are involved in abiotic stress responses (Yan et al. 2016; Zhang et al. 2018). In this study, we uncovered a function of miR165/166 in HS. We determined that the miR165/166–*PHB* module confers thermotolerance in *Arabidopsis* and revealed the underlying mechanism by which *HSFA1*-mediated transcriptional reprogramming is regulated by the miR165/166–*PHB* module to control plant responses to HS.

Results

HS triggers the accumulation of miR165/166, and overexpression of miR165/166 confers thermotolerance

The highly conserved miRNAs miR165 and miR166 play critical roles in plant development and response to abiotic stress. However, it is unclear whether they are involved in HS. We observed that HS treatment dramatically induced miR165/166 accumulation (Fig. 1, A and B), leading to lower transcript levels for its target genes *PHB* and *PHV* (Fig. 1C). To explore the potential role of miR165/166 in HS, we generated and selected 2 independent transgenic lines overexpressing miR165/166 with higher miR165/166 levels and compared their thermotolerance phenotype to that of the WT. Mature miR165/166 markedly accumulated to levels 10 to 20 times greater than WT levels in these transgenic lines, whereas the transcript levels of miR165/166 target genes dramatically decreased (Fig. 1, D and E). When 7-d-old seedlings were subjected to HS at 37°C, we observed that miR165/166 overexpression lines were more tolerant to HS than the WT (Figs. 1, F and G, and S1A). To confirm our findings, we generated a *phb phv* double mutant (Fig. 1H) and analyzed its thermotolerance phenotype. Compared to the WT, the *phb phv* double mutant exhibited higher tolerance to HS (Figs. 1, I and J, and S1B).

We also examined the thermotolerance of 3-wk-old soil-grown WT plants and miR165/166 overexpression lines subjected to HS at 37°C for 4 d. We observed less damage in miR165/166 overexpression lines than in WT plants (Supplemental Fig. S2). Similar to miR165/166 overexpression transgenic plants, the *phb phv* double mutant subjected to 37°C displayed a more tolerant phenotype (Supplemental Fig. S3). These results demonstrate that as miR165/166 accumulation increases in miR165/166 overexpression lines, the transcript levels of miR165/166 target genes decrease, resulting in enhanced thermotolerance.

Knockdown of miR165/166 makes plants more sensitive to HS

To investigate the role of miR165/166 in thermotolerance, we generated 2 moderate miR165/166 knockdown lines, STTM165/166, using the short tandem target mimicry (STTM) approach (Yan et al. 2012). The accumulation of miR165/166 in the STTM165/166 lines dropped by 70% relative to the WT control (Fig. 2A), whereas transcript levels for miR165/166 target genes were ~2 to 3.6 times higher than in WT (Fig. 2B). When 7-d-old WT and STTM165/166 seedlings were subjected to HS at 37°C, all STTM165/166 transgenic seedlings exhibited weaker thermotolerance than the WT

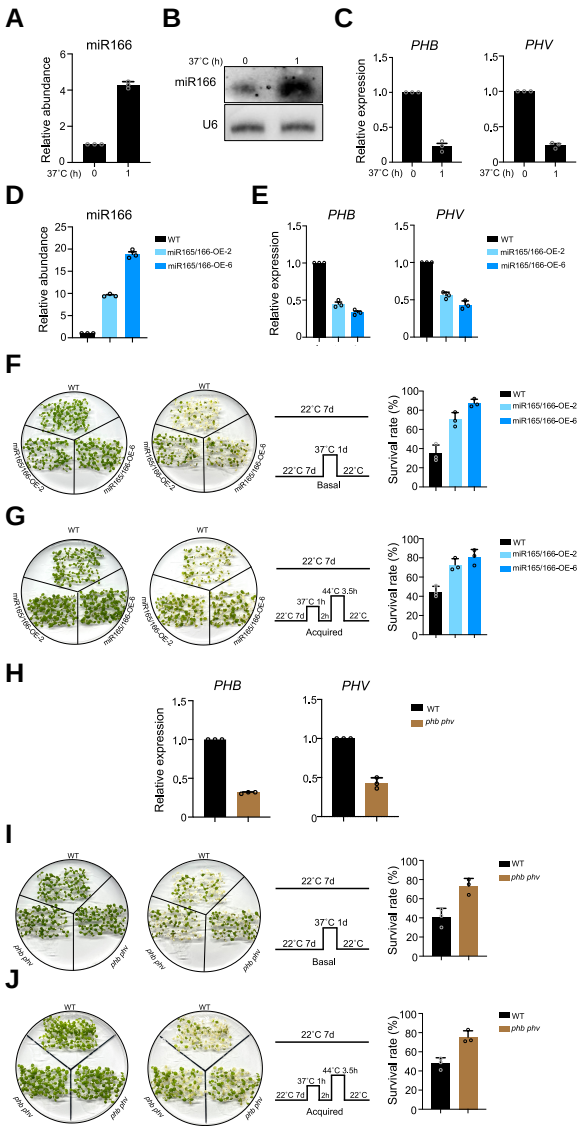

Figure 1. HS triggers the accumulation of miR165/166, and miR165/166 overexpression enhances plants thermotolerance. **A)** RT-qPCR analysis of mature miR166 levels in WT with or without 37°C treatment. SnoR101 was used as an internal control. Values are means ± SE from 3 independent biological replicates, with each data point indicated. **B)** Northern blot analysis of the abundance of mature miR166 in WT grown at 22°C or exposed to HS treatment at 37°C for 1 h. **C)** RT-qPCR analysis of transcript levels for miR166 target genes in WT grown at 22°C or exposed to HS treatment at 37°C for 1 h. *ACTIN* was used as an internal control. Values are means ± SE from 3 independent biological replicates, with each data point indicated. **D)** RT-qPCR analysis of mature miR166 abundance in WT and miR165/166 overexpression lines (miR165/166-OE). SnoR101 was used as an internal control. Values are means ± SE from 3 independent biological replicates, with each data point indicated. **E)** RT-qPCR analysis of miR166 target genes in WT and miR165/166-OE. *ACTIN* mRNA was used as an internal control. Values are means ± SE from 3 independent biological replicates, with each data point indicated. **F)** Basal thermotolerance analysis and survival rate of WT and miR165/166-OE after HS. Seven-day-old seedlings were exposed to 37°C for 1 d and allowed to recover at 22°C for 3 d. About 200 seedlings for each biological replicate were used, and 3 independent biological replicates were performed. Each biological replicate includes 4 technical

(continued)

control (Figs. 2, C and D, and S4A). These results suggest that lower levels of miR165/166 make seedlings more sensitive to HS.

We further explored this hypothesis using transgenic seedlings expressing a form of *PHB* that is resistant to miR165/166 cleavage, *PHBpro:PHBm-FLAG*. *PHB* transcript levels in these seedlings were much higher than those of WT (Fig. 2E), and *PHBpro:PHBm-FLAG* seedlings were more sensitive to HS compared to the WT (Fig. 2, F and G, and S4B). Consistent with these results, when 3-wk-old soil-grown WT and STTM165/166 and *PHBpro:PHBm-FLAG* plants were exposed to HS, the STTM165/166 and *PHBpro:PHBm-FLAG* plants displayed a severely damaged phenotype compared to the WT (Supplemental Figs. S5 and S6).

PHB represses the expression of *HSFA1s*

We investigated whether the miR165/166–*PHB* module regulates the expression of *HSFA1*s, which encode master regulators of HS responses. Surprisingly, expression analysis revealed that even at 22°C, *HSFA1* transcript levels were higher in miR165/166-OE lines compared to the WT control (Fig. 3A). After HS treatment of 1 h at 37°C, *HSFA1* transcript levels were still higher in miR165/166-OE lines compared to the WT (Fig. 3A). Similarly, in the *phb phv* double mutant, the expression of *HSFA1*s was higher relative to the WT regardless of HS treatment (Fig. 3B).

We next assayed the expression of *HSFA1*s in STTM165/166 lines and observed that their transcript levels were significantly lower than in the WT again regardless of HS

Figure 1. (Continued)
replicates of 50 seedlings. Values are means ± SE of 3 independent biological replicates, with each data point indicated. **G)** Acquired thermotolerance analysis and survival rate of WT and miR165/166-OE after HS. Seven-day-old seedlings were treated at 37°C for 1 h, returned to 22°C for 2 h, and then transferred to 44°C for 3.5 h and returned to 22°C for 3 d. About 200 seedlings for each biological replicate were used, and 3 independent biological replicates were performed. Each biological replicate includes 4 technical replicates. Values are means ± SE of 3 independent biological replicates, with each data point indicated. **H)** RT-qPCR analysis of transcript levels for miR166 target genes in WT and the *phb phv* double mutant. *ACTIN* was used as an internal control. Values are means ± SE from 3 independent biological replicates, with each data point indicated. **I)** Basal thermotolerance analysis and survival rate of WT and the *phb phv* double mutant after HS. Seven-day-old seedlings were exposed to 37°C for 1 d and allowed to recover at 22°C for 3 d. About 200 seedlings for each biological replicate were used, and 3 independent biological replicates were performed. Each biological replicate includes 4 technical replicates. Values are means ± SE of 3 independent biological replicates, with each data point indicated. **J)** Acquired thermotolerance analysis and survival rate of WT and the *phb phv* double mutant after HS. Seven-day-old seedlings were treated at 37°C for 1 h, returned to 22°C for 2 h, then transferred to 44°C for 3.5 h, and returned to 22°C for 3 d. About 200 seedlings for each biological replicate were used, and 3 independent biological replicates were performed. Each biological replicate includes 4 technical replicates. Values are means ± SE of 3 independent biological replicates, with each data point indicated.

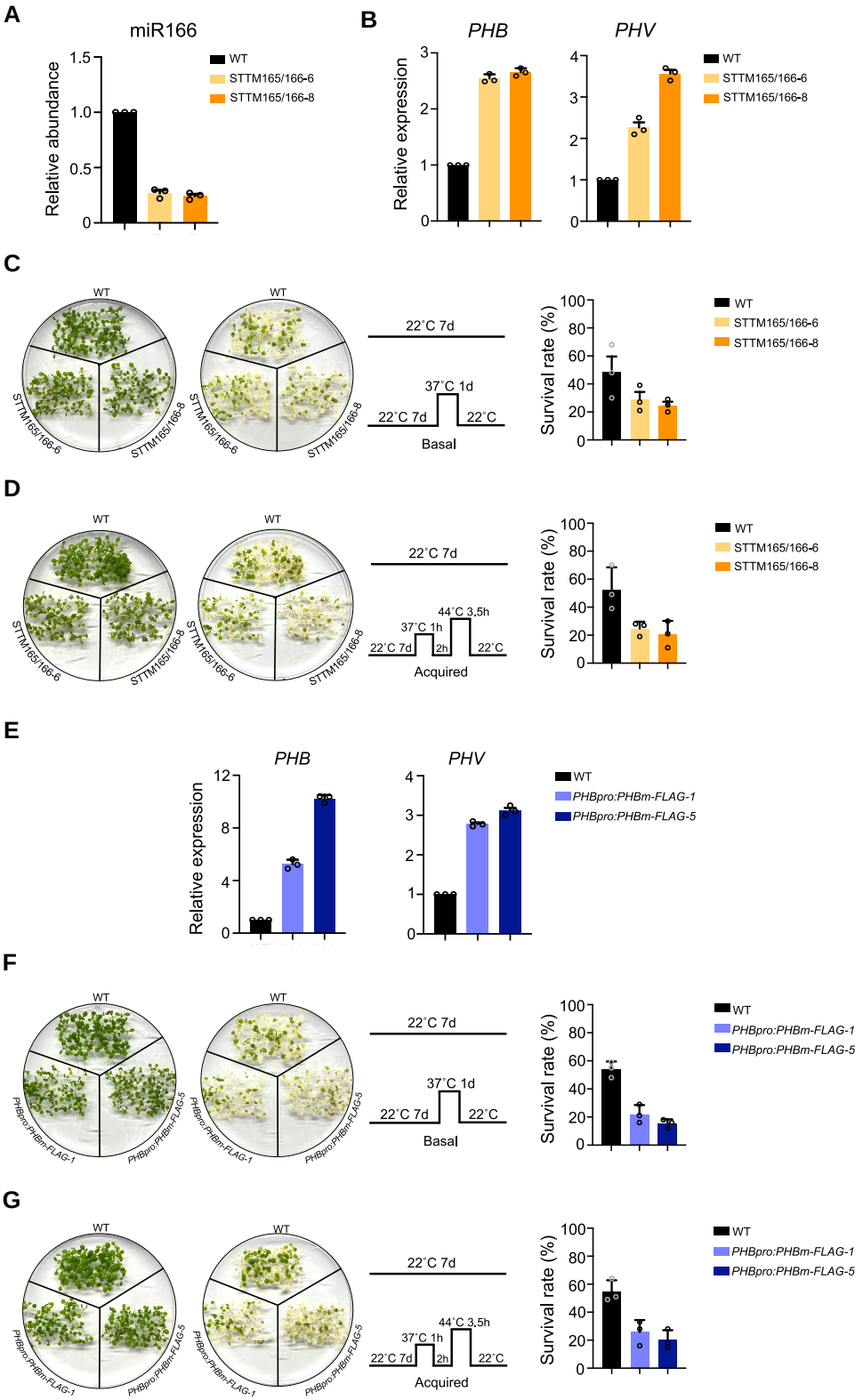

Figure 2. miR165/166 knockdown lines and *PHB* gain-of-function transgenic lines are more sensitive to HS. **A)** Analysis of mature miR166 abundance in WT and STTM165/166. SnoR101 was used as an internal control. Values are means ± SE from 3 independent biological replicates, with each data point indicated. **B)** Expression analysis of miR166 target genes in WT and STTM165/166. *ACTIN* mRNA was used as an internal control. Values are means ± SE from 3 independent biological replicates, with each data point indicated. **C)** Basal thermotolerance analysis and survival rate of WT and STTM165/166 after HS. Seven-day-old seedlings were exposed to 37°C for 1 d and allowed to recover at 22°C for 3 d. About 200 seedlings for each biological replicate were used, and 3 independent biological replicates were performed. Each biological replicate includes 4 technical

(continued)

treatment (Fig. 3C). Similarly, *HSFA1* transcript levels in the *PHBpro:PHBm-FLAG* transgenic lines were also lower relative to the WT grown at 22°C only or exposed to 37°C for 1 h (Fig. 3D). Together, these results demonstrate that the miR165/166–*PHB* module regulates the expression of *HSFA1*s.

*HSFA1*s are direct targets of PHB

To investigate whether PHB can directly modulate the expression of *HSFA1*s, we identified potential PHB protein-binding sites in the promoter regions of *HSFA1*s (Fig. 4A). Utilizing *PHBpro:PHBm-FLAG* transgenic plants, we performed a chromatin immunoprecipitation (ChIP) assay to examine whether PHB associates with *cis*-regulatory sequences containing these binding motifs in vivo. As shown in Fig. 4A, we detected PHB occupancy in the gene promoter regions of *HSFA1a* and *HSFA1b* where PHB binding motifs were located. An electrophoretic mobility shift assay (EMSA) further revealed the direct PHB binding to the enriched PHB recognition motif fragment (Figs. 4B and S7), demonstrating that *HSFA1a* and *HSFA1b* are 2 direct targets of PHB.

We performed a dual-luciferase (LUC) assay in *Nicotiana benthamiana* leaves to examine the effect of PHB on transcription from the *HSFA1a* and *HSFA1b* promoters, driving the firefly *LUC* reporter gene. Co-infiltration of the LUC reporters with *35S:PHB* decreased relative LUC activity, indicating that PHB negatively regulates the transcription of *HSFA1a* and *HSFA1b* (Figs. 4, C and D, and S8). We also performed a ChIP assay to examine whether PHB associates with the promoter regions of the other 2 members of the *HSFA1* family, *HSFA1d* and *HSFA1e*. As shown in Supplemental Fig. S9, we detected enrichment for the fragments containing the PHB recognition motif in the *HSFA1d* and *HSFA1e* promoter regions. These findings suggest that all 4 *HSFA1* members are targets of PHB, which acts as a transcriptional repressor in modulating their transcription.

Global gene expression analysis reveals that PHB represses *HSR* gene expression

To decipher the mechanism of thermotolerance mediated by the miR165/166–*PHB* module, we performed transcriptome deep sequencing (RNA-seq) on 7-d-old WT and *PHBpro:PHBm-FLAG* seedlings grown at 22°C or exposed to 37°C for 1 h (Fig. 5). Without HS treatment, 1,509 genes were upregulated, and 2,124 genes were downregulated in *PHBpro:PHBm-FLAG* transgenic seedlings compared to WT controls (Fig. 5A). The transcriptome of *PHBpro:PHBm-FLAG* transgenic seedlings differed even more from that of the WT after HS treatment, with the number of upregulated genes increasing from 1,509 to 1,628 and the number of downregulated genes rising from 2,124 to 2,456 (Fig. 5B). Gene ontology (GO) term enrichment analysis showed that downregulated genes in *PHBpro:PHBm-FLAG* transgenic seedlings are enriched in terms related to response to HS (Fig. 5D).

To validate our RNA-seq data, we chose several *HSP* genes such as *HSP90-1*, *HSP17.6B*, *HSP17.4B*, *HSP101*, *HSP17.4*, and *HSP17.6C* for reverse transcription quantitative PCR (RT-qPCR) analysis. The expression levels of these genes were significantly lower in *PHBpro:PHBm-FLAG* seedlings relative to WT regardless of HS treatment (Figs. 5E and S10). We also examined the transcript levels of these genes in STTM165/166 and miR165/166-OE lines, which revealed their downregulation in STTM165/166 lines and their upregulation in miR165/166-OE lines compared to the WT control with or without HS treatment (Figs. 5E and S10). Together, these results indicate that PHB is involved in the transcriptional reprogramming of gene expression in response to HS.

HSFA2 is a common target of both HSFA1s and PHB

The above RNA-seq analysis revealed that the expression of the essential *HSR* gene regulator *HSFA2* was lower in *PHBpro:PHBm-FLAG* transgenic seedlings compared to that of the WT with or without HS treatment. We conducted an RT-qPCR analysis to explore whether *HSFA2* is regulated by the miR165/166–*PHB* module. *HSFA2* mRNA abundance clearly decreased in *PHBpro:PHBm-FLAG* and STTM165/166 transgenic lines and dramatically increased in miR165/166-OE lines compared to the WT, regardless of HS treatment (Fig. 6A). Promoter sequence analysis indicated that the *HSFA2* promoter contains a PHB recognition motif (Fig. 6B). To investigate whether PHB might directly regulate *HSFA2* transcription, we performed a ChIP assay and EMSAs and

Figure 2. (Continued)
replicates. Values are means ± SE from 3 independent biological replicates, with each data point indicated. **D)** Acquired thermotolerance analysis and survival rate of WT and STTM165/166 after HS. Seven-day-old seedlings were treated at 37°C for 1 h, returned to 22°C for 2 h, then transferred to 44°C for 3.5 h, and returned to 22°C for 3 d. About 200 seedlings for each biological replicate were used, and 3 independent biological replicates were performed. Each biological replicate includes 4 technical replicates. Values are means ± SE from 3 independent biological replicates, with each data point indicated. **E)** Expression analysis of transcript levels for miR166 target genes in WT and *PHBpro:PHBm-FLAG* (a miR165/166 cleavage-resistant version) transgenic lines. *ACTIN* was used as an internal control. Values are means ± SE from 3 independent biological replicates, with each data point indicated. **F)** Basal thermotolerance analysis and survival rate of WT and *PHBpro:PHBm-FLAG* transgenic lines after HS. Seven-day-old seedlings were exposed to 37°C for 1 d and allowed to recover at 22°C for 3 d. About 200 seedlings for each biological replicate were used, and 3 independent biological replicates were performed. Each biological replicate includes 4 technical replicates. Values are means ± SE from 3 independent biological replicates, with each data point indicated. **G)** Acquired thermotolerance analysis and survival rate of WT and *PHBpro:PHBm-FLAG* after HS. Seven-day-old seedlings were treated at 37°C for 1 h, returned to 22°C for 2 h, then transferred to 44°C for 3.5 h, and returned to 22°C for 3 d. About 200 seedlings for each biological replicate were used, and 3 independent biological replicates were performed. Each biological replicate includes 4 technical replicates. Values are means ± SE from 3 independent biological replicates, with each data point indicated.

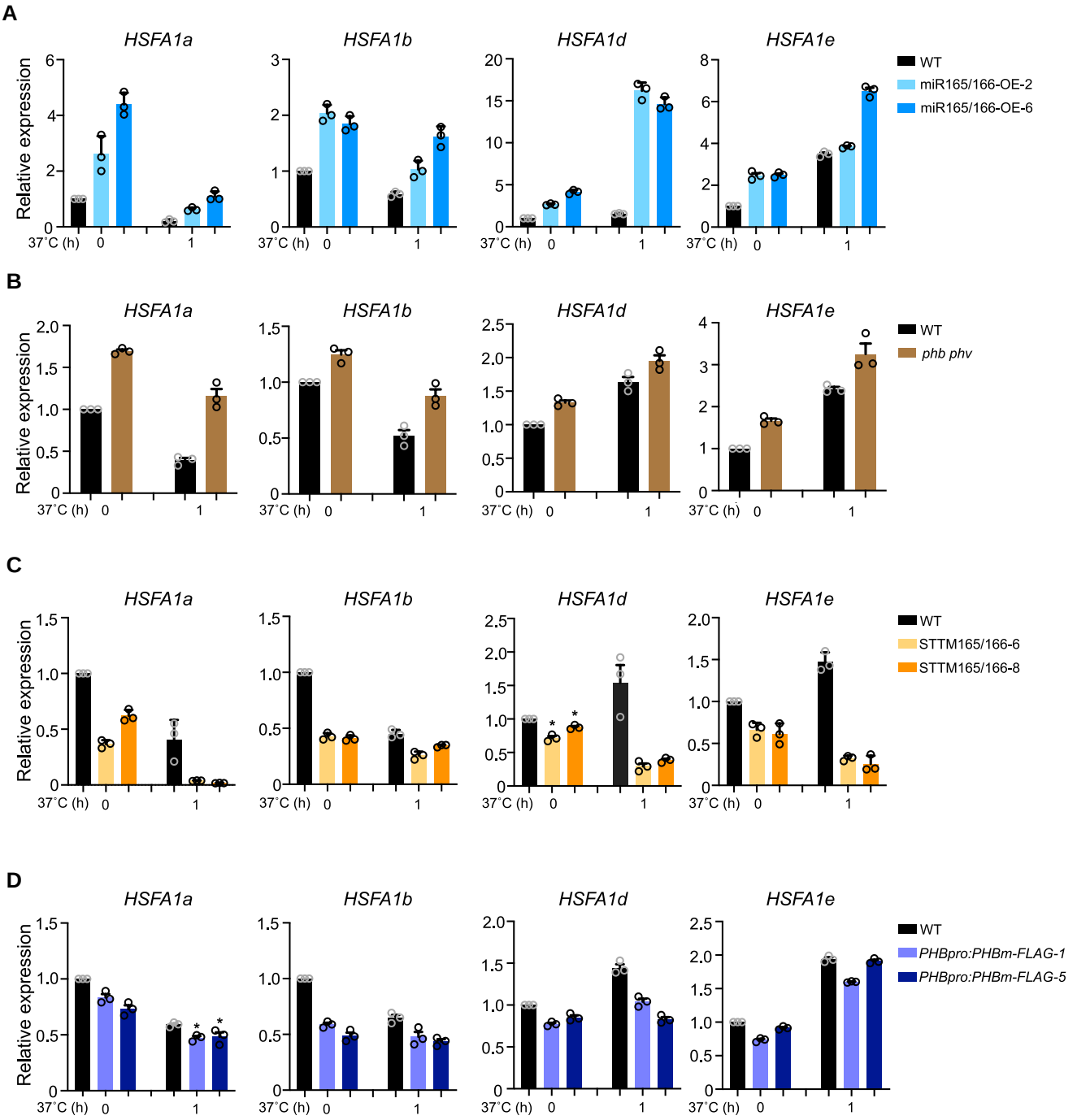

Figure 3. The miR165/166–*PHB* module affects the expression of *HSFA1*s. **A)** Expression levels of *HSFA1*s in WT and miR165/166-OE grown at 22°C or exposed to HS treatment at 37°C for 1 h. *ACTIN* was used as an internal control. Values are means ± SE from 3 independent biological replicates, with each data point indicated. **B)** Expression levels of *HSFA1*s in WT and the *phb phv* double mutant grown at 22°C or exposed to HS treatment at 37°C for 1 h. *ACTIN* was used as an internal control. Values are means ± SE from 3 independent biological replicates, with each data point indicated. **C)** Expression levels of *HSFA1*s in WT and STTM165/166 grown at 22°C or exposed to HS treatment at 37°C for 1 h. *ACTIN* was used as an internal control. Values are means ± SE from 3 independent biological replicates, with each data point indicated. Significant differences were analyzed by ANOVA (*$P < 0.05$). **D)** Expression levels of *HSFA1*s in WT and *PHBpro:PHBm-FLAG* (a miR165/166 cleavage-resistant version) grown at 22°C or exposed to HS treatment at 37°C for 1 h. *ACTIN* was used as an internal control. Values are means ± SE from 3 independent biological replicates, with each data point indicated. Significant differences were analyzed by ANOVA (*$P < 0.05$).

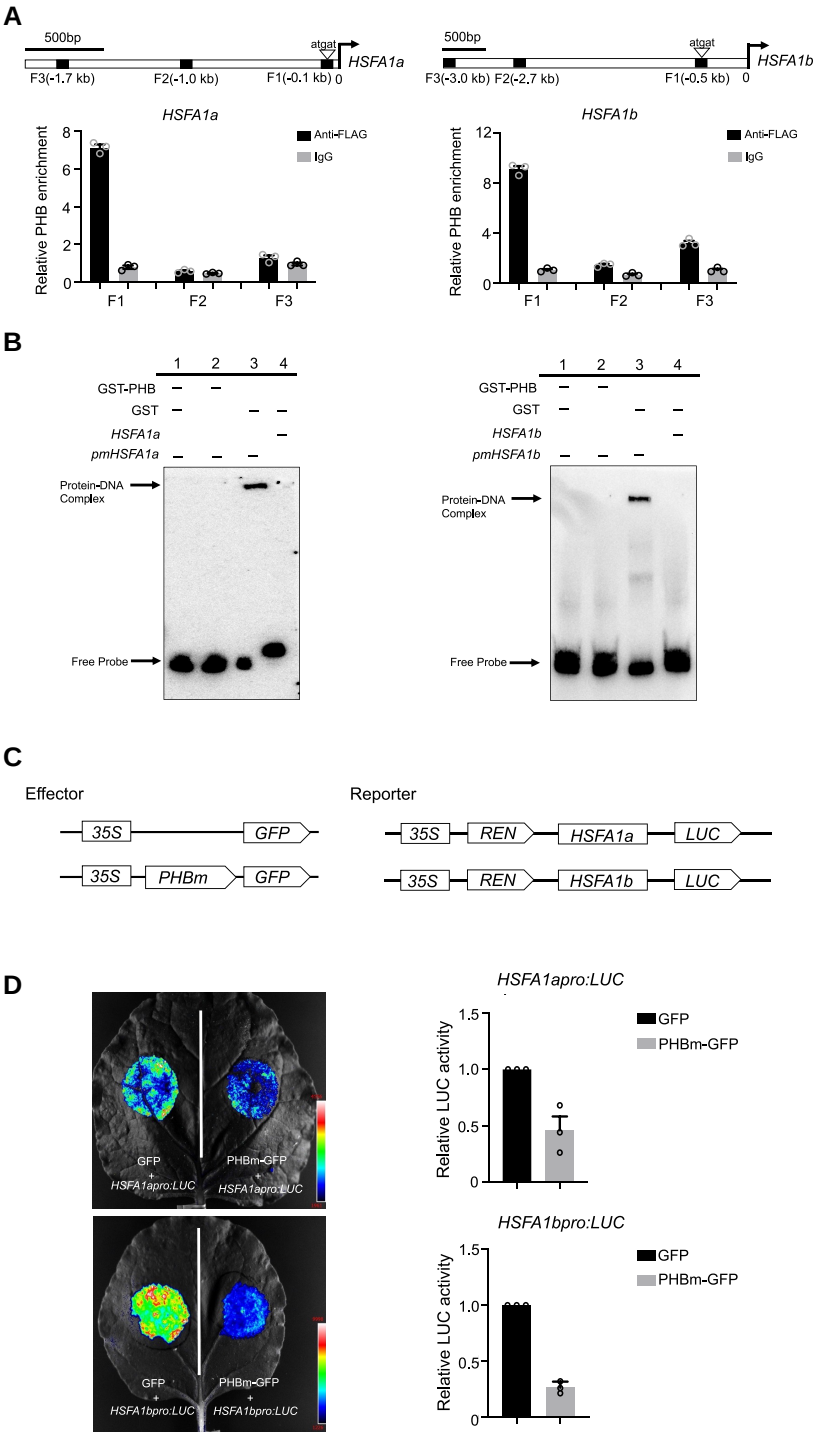

Figure 4. PHB directly binds to the promoters of *HSFA1*s and inhibits their transcription. **A)** Top: schematic diagrams of the promoter regions of *HSFA1a* and *HSFA1b*. Arrowheads indicate the positions of the core sequence (5′-atgat-3′) for the PHB recognition motif. Squares indicate the fragments amplified in ChIP-qPCR. Bottom: *PHBpro:PHBm-FLAG* seedlings were used for ChIP-qPCR, and IgG was used as the negative control. Values are means ± SE from 3 independent biological replicates, with each data point indicated. **B)** EMSA showing the direct binding of PHB to promoter regions of *HSFA1a* and *HSFA1b*. The positions of the DNA–protein complex and free probe are marked. The biotin-labeled probes containing the PHB recognition motif were incubated with GST-PHB recombinant proteins. The GST lane and mutated version of probes (*pmHSFA1a* and *pmHSFA1b*) lane were used as negative control. **C)** Schematic diagrams of effectors and reporters used in the transient dual-LUC reporter assay. Expression of *PHB* and *REN* was driven by the *35S* promoter. The *LUC* reporter gene was driven by the *HSFA1a* or *HSFA1b* native promoter. **D)** Transient dual-LUC reporter assay in *N. benthamiana* leaves showing that PHB suppresses the promoter activity of *HSFA1a* and *HSFA1b*. Relative LUC activity was normalized to REN activity. Values are means ± SE from 3 independent biological replicates, with each data point indicated. For each replicate, at least 3 batches of plants were tested.

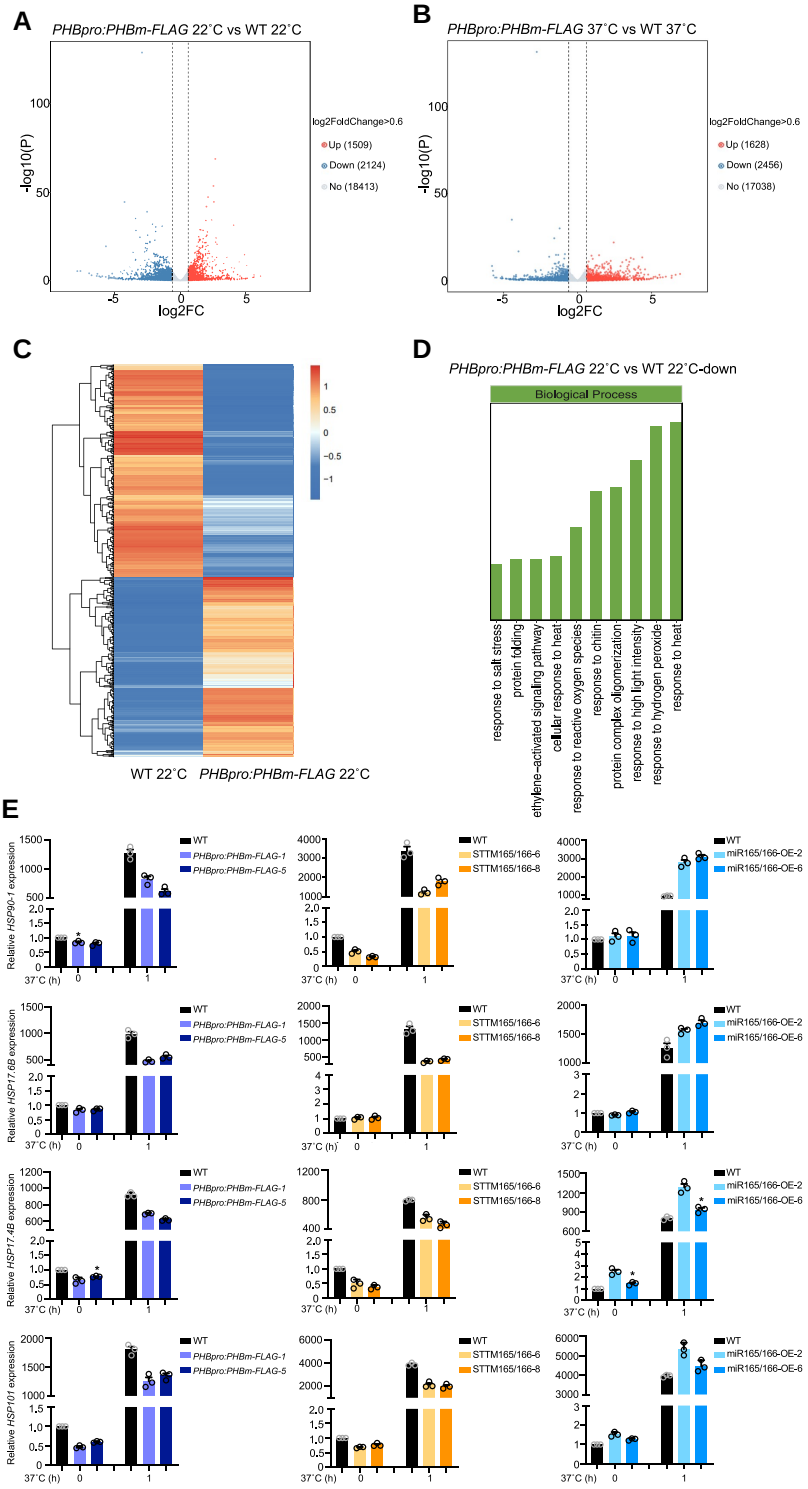

Figure 5. Transcriptome profiling of WT and *PHBpro:PHBm-FLAG* seedlings with or without HS. **A)** Volcano plot showing gene expression in WT and *PHBpro:PHBm-FLAG* grown at 22°C. Blue dots, downregulated genes; red dots, upregulated genes; gray dots, no change. **B)** Volcano plot showing gene expression in WT and *PHBpro:PHBm-FLAG* that were both exposed to 1 h of 37°C treatment. Blue dots, downregulated genes; red dots, upregulated genes; gray dots, no change. **C)** Heatmap of the transcriptome data from WT and *PHBpro:PHBm-FLAG* grown at 22°C. Red, upregulation; blue, downregulation; white, no change. The color scale represents the relative level of expression, which is normalized by the *Z*-score algorithm. Red, high *Z*-scores; blue, low *Z*-scores. **D)** GO enrichment analysis for downregulated genes in *PHBpro:PHBm-FLAG* compared to WT. **E)** *HSP* gene expression analysis in WT, *PHBpro:PHBm-FLAG*, STTM165/166, and miR165/166-OE grown at 22° or exposed to HS treatment at 37°C for 1 h. *ACTIN* was used as an internal control. Values are means ± SE from 3 independent biological replicates, with each data point indicated. Significant differences were analyzed by ANOVA (*$P < 0.05$).

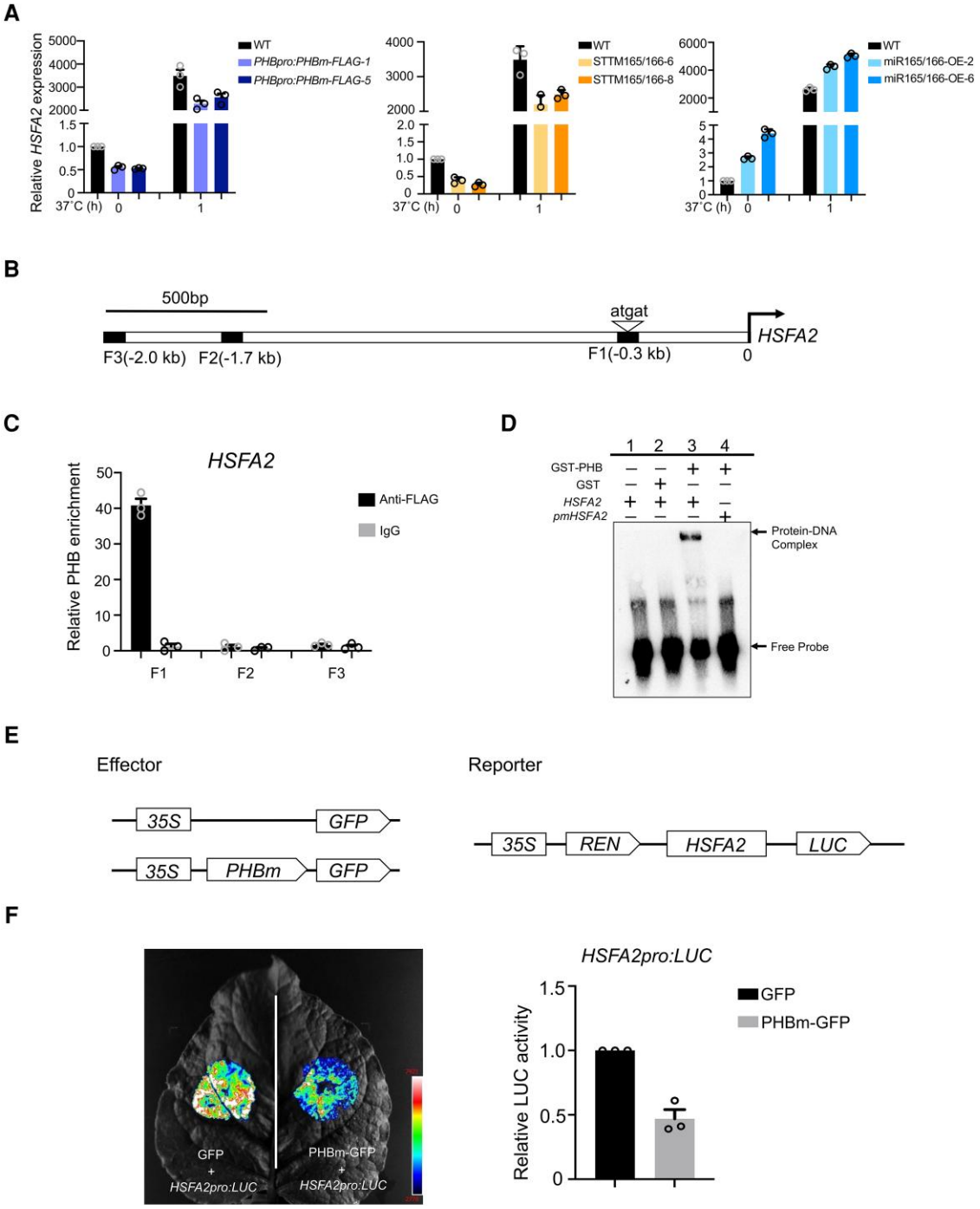

Figure 6. *HSFA2* is a direct target of PHB. **A)** Expression analysis of *HSFA2* in WT, *PHBpro:PHBm-FLAG*, STTM165/166, and miR165/166-OE grown at 22°C or exposed to HS treatment at 37°C for 1 h. *ACTIN* was used as an internal control. Values are means ± SE from 3 independent biological replicates, with each data point indicated. **B)** Schematic diagram of the *HSFA2* promoter region. The arrowhead indicates the position of the core sequence (5′-atgat-3′) for the PHB recognition motif. Squares indicate the fragments amplified in ChIP-qPCR. **C)** ChIP-qPCR analysis of PHB binding to the *HSFA2* promoter. *PHBpro:PHBm-FLAG* seedlings were used for ChIP-qPCR, and IgG was used for the negative control. Values are means ± SE from 3 independent biological replicates, with each data point indicated. **D)** EMSA showing the direct binding of PHB to promoter regions of *HSFA2*. The positions of the DNA–protein complex and free probe are marked. The biotin-labeled probe containing the PHB recognition motif was incubated with recombinant GST-PHB. GST lane and mutated version of probes (*pmHSFA2*) lane were used for negative control. **E)** Schematic diagrams of effectors and reporters used in the transient dual-LUC reporter assay. Expression of *PHB* and *REN* was driven by the *35S* promoter. The *LUC* reporter gene was driven by the *HSFA2* native promoter. **F)** Transient dual-LUC reporter assay in *N. benthamiana* leaves showing that PHB suppresses the promoter activity of *HSFA2*. Relative LUC activity was normalized to REN activity. Values are means ± SE from 3 independent biological replicates, with each data point indicated. For each replicate, at least 3 batches of plants were determined.

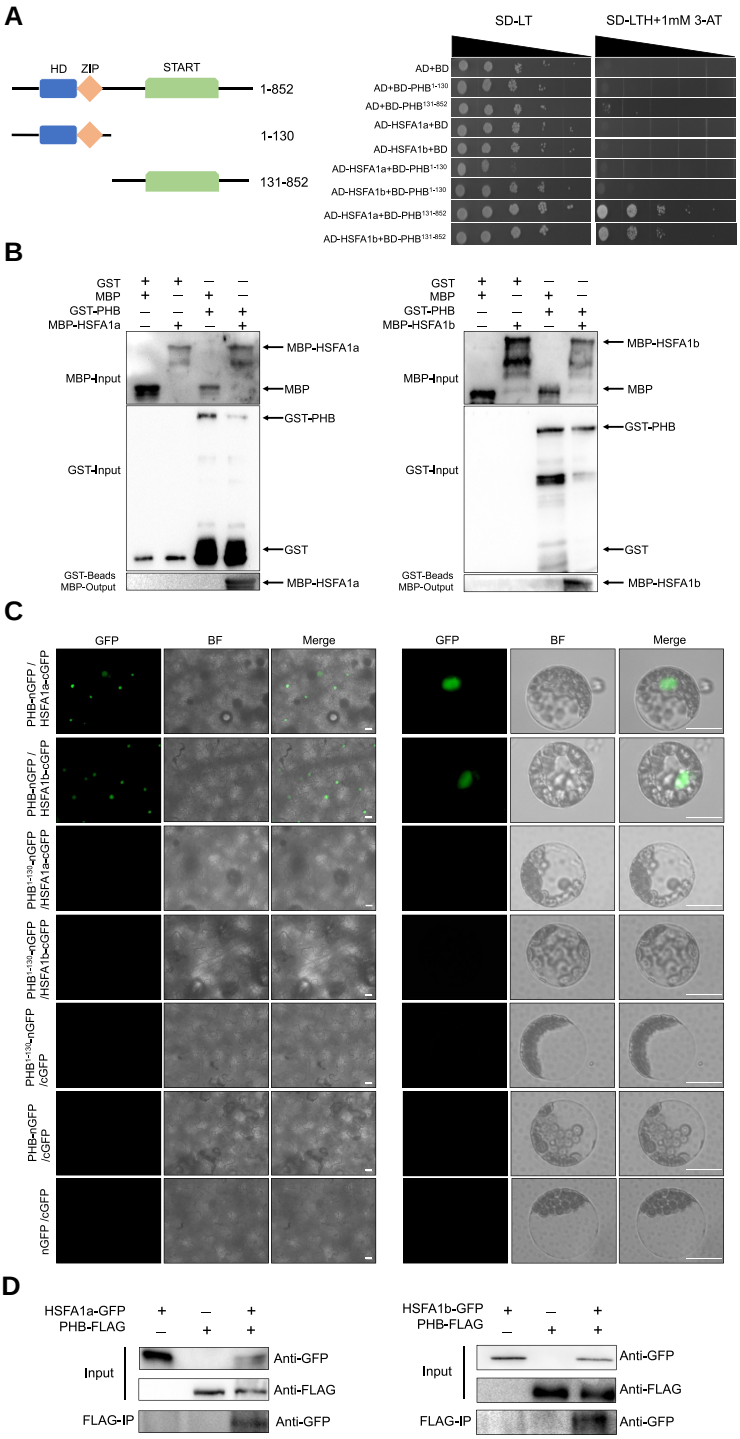

Figure 7. PHB directly interacts with HSFA1a or HSFA1b. **A)** Yeast 2-hybrid assays showing the interaction between PHB and HSFA1a or HSFA1b. Left, schematic diagram showing the functional domains of PHB: START, steroidogenic acute regulatory protein-related lipid transfer domain; HD, homeodomain; ZIP, leucine zipper. –LT, synthetic defined (SD) medium lacking leucine and tryptophan; –LTH, SD medium lacking leucine, tryptophan, and histidine. 3-amino-1,2,4-triazole (3-AT) was added to the medium to reduce autoactivation. **B)** In vitro pull-down assays showing the interaction between PHB and HSFA1a or HSFA1b. Recombinant MBP-HSFA1a or MBP-HSFA1b was pulled down by GST-PHB and detected by anti-MBP antibody. **C)** BiFC assays showing that PHB physically interacts with HSFA1a or HSFA1b, whereas PHB^{1-130} lacking an interaction domain does not, in *N. benthamiana* leaves and *Arabidopsis* protoplasts. The fluorescence signal was captured by Zeiss Imager A2. Scale bars, 50 μm. **D)** Co-IP assays showing the interaction between PHB and HSFA1a or HSFA1b. *PHB-FLAG* was co-infiltrated with *HSFA1a-GFP* or *HSFA1b-GFP* in *N. benthamiana* leaves. PHB-FLAG protein was immunoprecipitated with anti-FLAG antibodies mixed with protein A/G agarose beads, and the immunoprecipitated HSFA1a-GFP or HSFA1b-GFP was then detected using an anti-GFP antibody.

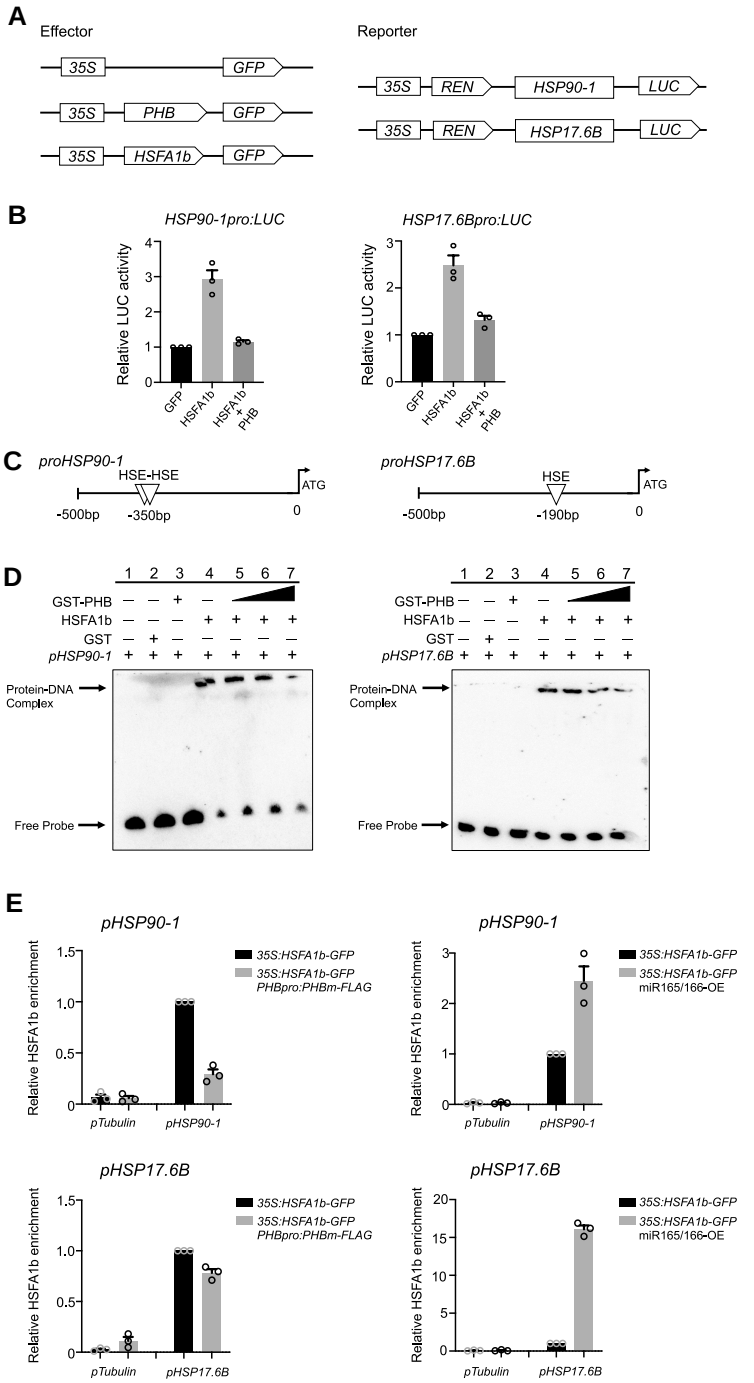

Figure 8. PHB interferes with the transcriptional function of HSFA1b. **A)** Schematic diagrams of the effectors and reporters used in the transient dual-LUC reporter assay. The expression of *PHB*, *HSFA1b*, or *REN* was driven by the *35S* promoter. The *LUC* reporter gene was driven by the native promoter of *HSP90-1* or *HSP17.6B*. **B)** Transient dual-LUC reporter assays in *N. benthamiana* leaves showing that PHB has an antagonistic effect on HSFA1b for the regulation of *HSP90-1* or *HSP17.6B* transcription. Relative LUC activity was normalized to REN activity. Values are means ± SE from 3 independent biological replicates, with each data point indicated. For each replicate, at least 3 batches of plants were determined. **C)** Schematic diagrams of the promoter regions of *HSP90-1* and *HSP17.6B*. Triangles indicate the position of the HSE element for HSFA1s recognition. **D)** EMSA showing that PHB antagonizes HSFA1b binding to the promoters of *HSP90-1* and *HSP17.6B*. The position of DNA–protein complex and free probe are marked. The biotin-labeled probe containing the HSE element was incubated with recombinant GST-PHB or MBP-HSFA1b. **E)** ChIP-qPCR analysis showing that the DNA binding of HSFA1b to the HSE element at the promoters of *HSP90-1* and *HSP17.6B* is inhibited by PHB. Seven-day-old seedlings of *35S:HSFA1b-GFP*, *35S:HSFA1b-GFP PHBpro:PHBm-FLAG*, and *35S:HSFA1b-GFP* miR165/166-OE were used. qPCR data with the *TUBULIN* promoter (*TUBpro*) as a negative control. Values are means ± SE from 3 independent biological replicates, with each data point indicated.

determined that PHB directly binds to the *HSFA2* promoter (Figs. 6, C and D, and S11). Given that HSFA1s can directly regulate *HSFA2* transcription, these findings indicate that *HSFA2* serves as a common target of both HSFA1s and PHB.

We also conducted a dual-LUC assay in *N. benthamiana* leaves and found that the activity of the *HSFA2pro:LUC* reporter was substantially lower when co-infiltrating the effector construct *35S:PHB*, supporting the negative role of PHB in the regulation of *HSFA2* transcription (Figs. 6, E and F, and S12).

PHB physically interacts with HSFA1s

Given that the activity of HSFA1s is strictly controlled by protein–protein interactions, we investigated the possibility of direct interactions between PHB and the HSFA1 members HSFA1a and HSFA1b using a yeast 2-hybrid assay. Indeed, the C-terminal region, but not the N-terminal region of PHB, physically interacted with HSFA1a and HSFA1b (Fig. 7A). To validate this interaction, we conducted an in vitro pull-down assay using maltose-binding protein (MBP)-tagged HSFA1a or HSFA1b as a prey and glutathione S-transferase (GST)-tagged PHB as a bait. GST-tagged PHB, but not the control protein GST, interacted with HSFA1a and HSFA1b (Fig. 7B).

We obtained further support for the interactions between PHB, HSFA1a, and HSFA1b by bimolecular fluorescence complementation (BiFC) assays. We generated constructs encoding PHB fused to the N-terminus of green fluorescent protein (GFP), while HSFA1a and HSFA1b were individually fused to the C-terminus of GFP. We then co-infiltrated the appropriate pairs of constructs into *N. benthamiana* leaves. Although we observed strong GFP fluorescence in the nucleus, we detected no signal in the negative controls (Fig. 7C). We confirmed this result in *Arabidopsis* protoplasts transfected with the same constructs (Fig. 7C).

To further validate the interaction between PHB and HSFA1s, we performed co-immunoprecipitation (co-IP) assays by co-expressing *PHB-FLAG* and *HSFA1a-GFP* or *HSFA1b-GFP* in *N. benthamiana*. We determined that HSFA1a or HSFA1b can be clearly pulled down by PHB (Fig. 7D). Together, these findings suggest that PHB can physically interact with HSFA1a and HSFA1b.

PHB interferes with HSFA1 activity for binding to their targets

To determine whether direct interactions between PHB and HSFA1s affect transcriptional activity of the latter, we performed a dual-LUC assay where the expression of both *HSFA1b* and *PHB* was driven by the *35S* promoter (Fig. 8A). For the assay, we selected the promoters of *HSP90-1* and *HSP17.6B*, as they harbor only the binding sites for HSFA1s, but not the PHB recognition motif. LUC activity derived from the *HSP90-1pro:LUC* and *HSP17.6Bpro:LUC* reporter constructs was dramatically stimulated upon co-expression of *HSFA1b* (Fig. 8B). By contrast, the co-expression of *HSFA1b* and *PHB* repressed relative LUC activity compared to when *HSFA1b* was expressed (Fig. 8B). These findings indicate that PHB interferes with HSFA1b transcriptional function.

We performed an EMSA to test whether PHB affects the binding activity of HSFA1b to an oligonucleotide containing the HSE motif. As shown in Figs. 8, C and D, and S13, HSFA1b did bind to the *cis*-element; however, when recombinant PHB was added, the binding of HSFA1b to the *cis*-element dramatically decreased. We performed a ChIP assay to examine the effects of PHB on the binding of HSFA1b to the promoters of *HSP90-1* and *HSP17.6B* in vivo. Compared to *35S:HSFA1b-GFP* seedlings, the enrichment of HSFA1b at the promoters of *HSP90-1* and *HSP17.6B* was lower in *35S:HSFA1b-GFP PHBpro:PHBm-FLAG* seedlings (Fig. 8E), which we generated by crossing *35S:HSFA1b-GFP* and *PHBpro:PHBm-FLAG* transgenic lines, therefore maintaining similar expression levels for *HSFA1b* (Supplemental Fig. S14, A and B). However, in the *35S:HSFA1b-GFP* miR165/166-OE lines, which we obtained by crossing *35S:HSFA1b-GFP* and miR165/166-OE lines and thus maintain similar *HSFA1b* expression levels as the single transgenic lines (Supplemental Fig. S14, C and D), the enrichment of HSFA1b at the promoters of *HSP90-1* and *HSP17.6B* was enhanced compared to *35S:HSFA1b-GFP* seedlings (Fig. 8E). These findings indicate that PHB disrupts the DNA binding of HSFA1b and has an antagonistic effect on HSFA1b in the regulation of *HSR* gene expression.

PHB mediates the HSFA1-triggered transcriptional reprogramming upon HS

HSFA1s function as master regulators in the activation of *HSR* transcriptional networks, whereas PHB has an antagonistic effect on the regulation by HSFA1s. We hypothesized that the transcriptional reprogramming triggered by *HSFA1s* upon HS might be mediated by PHB. Accordingly, we compared the transcriptome profile between HS-treated *PHBpro:PHBm-FLAG* seedlings and the HS-treated *hsfa1a hsfa1b hsfa1d hsfa1e* quadruple mutant, which was generated in the Col-0 genetic background (Fig. 9A). After HS treatment, we identified 3,989 genes regulated by HSFA1s (quadruple mutant compared to WT) and 4,084 genes regulated by PHB (*PHBpro:PHBm-FLAG* relative to WT) (Fig. 9B). Almost half of these genes (1,945 genes) were co-regulated by HSFA1s and PHB. In all, 733 genes and 809 genes were upregulated or downregulated, respectively, in both the *hsfa1* quadruple mutant and *PHBpro:PHBm-FLAG* seedlings (Fig. 9B). Importantly, for the subset of 1,945 genes co-regulated by HSFA1s and PHB, most (1,517 of 1,945) including many *HSP*s displayed HS-triggered alterations in expression (WT HS-treated compared to WT untreated) (Fig. 9, C and D). Collectively, these data indicate that PHB plays a crucial role in mediating the HSFA1-triggered transcriptome reprogramming during HS.

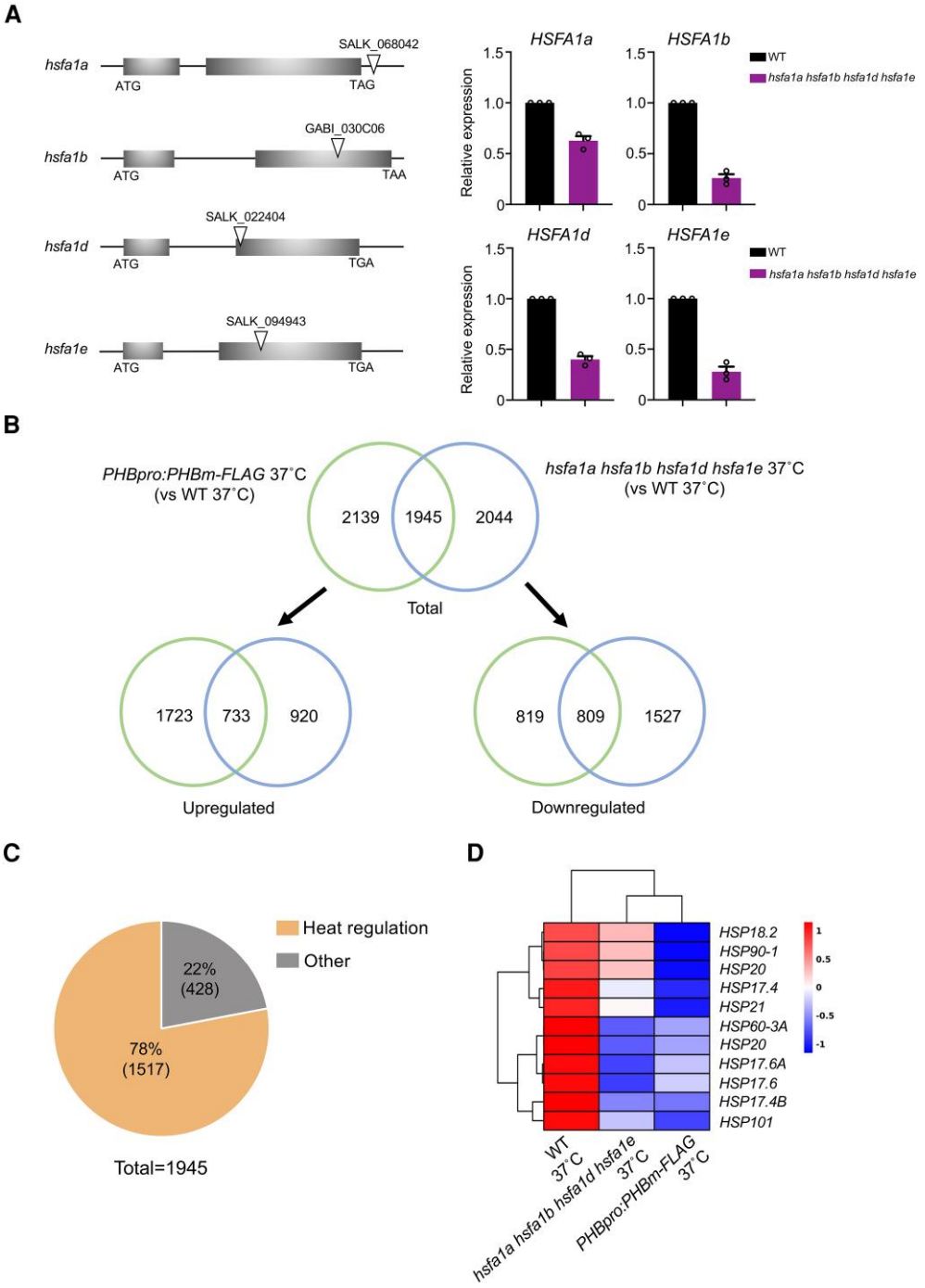

Figure 9. The miR165/166–*PHB* module plays an important role in plant HS pathway. **A)** Left: structures of *HSFA1* loci and the position of the T-DNA insertions marked by triangles. Boxes indicate exons. Right, RT-qPCR analysis of the transcript levels of *HSFA1* genes. Values are means ± SE from 3 independent biological replicates, with each data point indicated. **B)** Venn diagrams showing the extent of overlap between the sets of DEGs regulated by PHB (*PHBpro:PHBm-FLAG* 37°C relative to WT 37°C) compared to DEGs regulated by HSFA1s (quadruple mutant 37°C relative to WT 37°C). In total, 1,945 genes were co-regulated by HSFA1s and PHB. Among these genes, the changes of 1,542 genes are in the same trend in the *hsfa1* quadruple mutant and *PHBpro:PHBm-FLAG* seedlings. A total of 733 genes and 809 genes were upregulated or downregulated, respectively, in both the *hsfa1* quadruple mutant and *PHBpro:PHBm-FLAG* seedlings. The changes of the remaining 403 genes are in opposite trend in the *hsfa1* quadruple mutant and *PHBpro:PHBm-FLAG* seedlings. **C)** Percentage of heat-regulated genes among co-regulated genes in *PHBpro:PHBm-FLAG* and *hsfa1a hsfa1b hsfa1d hsfa1e* after 37°C treatment. Of the 1,945 co-regulated genes, ∼78% (1517 of 1945) are associated with the heat response. **D)** Heatmap of *HSP* genes in WT, *hsfa1a hsfa1b hsfa1d hsfa1e*, and *PHBpro:PHBm-FLAG* with 37°C treatment. Red, upregulation; blue, downregulation; white, no change. The color scale represents the relative level of expression, which is normalized by the *Z*-score algorithm. Red, high *Z*-scores; blue, low *Z*-scores.

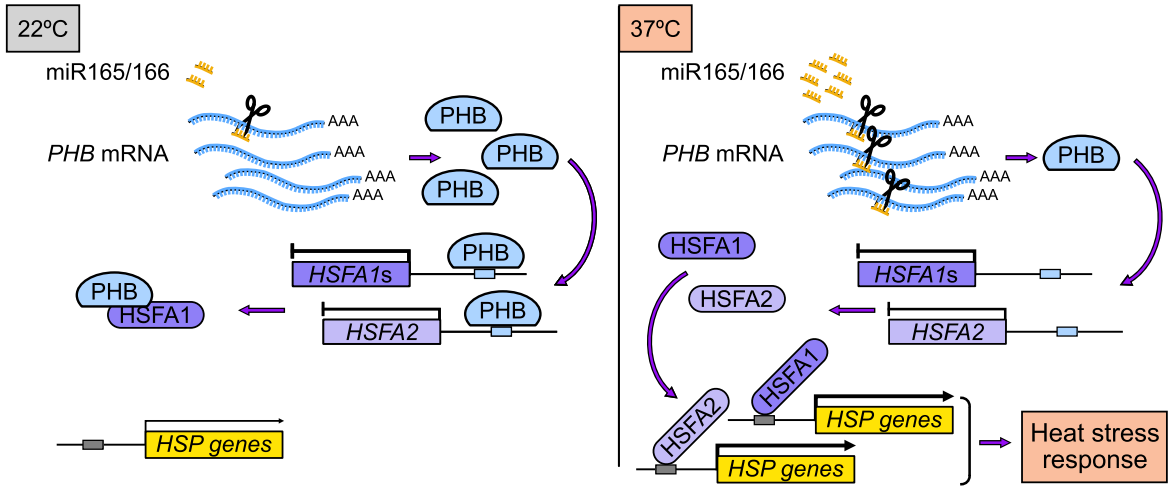

Figure 10. A working model for the transcriptional reprogramming mediated by the miR165/166–*PHB* module to regulate plant thermotolerance. HS triggers the accumulation of miR165/166, leading to the downregulation of its target genes. The miR165/166–*PHB* module regulates thermotolerance through at least 2 pathways. One is through direct transcriptional regulation of *HSF*s. PHB can modulate the transcription of *HSR*s in an *HSFA1*-dependent manner. PHB can also regulate the transcription of *HSR*s in an *HSFA1*-independent manner by directly regulating the transcription of heat-inducible *HSFA2*. In addition, PHB physically interacts with HSFA1s and interferes with their transcription function.

The miR165/166–*PHB* module acts upstream of *HSFA1*s genetically in the control of thermotolerance

Given that the activity of HSFA1s can be regulated by the miR165/166–*PHB* module, we investigated the genetic relationship between *HSFA1*s and the miR165/166–*PHB* module in the regulation of HS responses. To this end, we compared the thermotolerance phenotype of miR165/166-OE lines and miR165/166-OE lines in the *hsfa1a hsfa1b hsfa1d* mutant background. Although the expression level of miR165/166 target genes was similar in miR165/166-OE and *hsfa1a hsfa1b hsfa1d* miR165/166-OE (Supplemental Fig. S15A), we observed that the stronger thermotolerance phenotype of miR165/166-OE lines is suppressed when assessed in the *hsfa1a hsfa1b hsfa1d* mutant background (Supplemental Fig. S15B). Thus, the miR165/166–*PHB* module acts upstream of *HSFA1*s genetically in the regulation of thermotolerance.

Discussion

In this study, we identified miR165/166 as essential to the HS response and provided evidence that the miR165/166–*PHB* module contributes greatly to HS response in *Arabidopsis* (Fig. 10). The miR165/166 knockdown transgenic lines, STTM165/166, and *PHBpro:PHBm-FLAG* plants are hypersensitive to HS (Fig. 2, C and D and F and G). By contrast, the miR165/166 overexpression lines and the *phb phv* double mutant are more tolerant of HS (Fig. 1, F and G and I and J). We determined that the miR165/166–*PHB* module influences the expression of *HSFA1* genes and that PHB can bind to the promoter regions of *HSFA1*s to inhibit their transcription (Figs. 3 and 4). RNA-seq analysis revealed that PHB-mediated thermotolerance involves suppression of *HSR* gene expression (Fig. 5, D and E). In addition, we identified *HSFA2* as a common target of PHB and HSFA1s (Fig. 6). Our work revealed that PHB directly interacts with HSFA1s (Fig. 7) and has an antagonistic effect on their binding to the promoters of *HSR* genes, thereby interfering with the transcriptional function of HSFA1s (Fig. 8). Transcriptome profile comparison between the *hsfa1* quadruple mutant and *PHBpro:PHBm-FLAG* seedlings upon HS further reinforced the idea that PHB is involved in global transcriptional reprogramming by HSFA1s during HS (Fig. 9). Our data thus reveal the miR165/166–*PHB* module as an important positive regulator for thermotolerance and show how the miR165/166–*PHB* module controls plant response to HS by regulating *HSFA1*-mediated transcriptional reprogramming during HS (Fig. 10).

The highly conserved HSFs act as central regulators of *HSR* genes in both animals and plants. In plants, HSFA1s are the master regulator and activate the HSR gene expression upon HS (Jones-Rhoades et al. 2006; Reyes and Chua 2007; Ohama et al. 2017). Notably, unlike *HSFA2*, which is 1 of the HS-inducible *HSF*s, the effect of overexpressing *HSFA1*s is relatively limited, because HSFA1s activity is strictly controlled at the posttranslational level. Protein–protein interactions are important for regulation of and by HSFA1s. Previous studies have shown that HSP70 and HSP90 physically interact with HSFA1s and negatively regulate their activity by modulating their nuclear localization and transactivation activity (Fujii et al. 2009; Smith and Long 2010; Ohama et al. 2017). In this work, we revealed that PHB physically interacts with HSFA1s and has an antagonistic effect on their regulation of *HSR* gene expression at the posttranslational level. In *Arabidopsis*, the HSFA1 members HSFA1a, HSFA1b, and HSFA1d can physically interact with one another and appear to function as homocomplexes or heterocomplexes (Yoshida et al. 2011). The interaction of PHB with HSFA1s might interfere with the formation of

such functional HSFA1s complexes, and the competition between PHB and HSFA1s will affect the binding ability of HSFA1s to the promoters of *HSR* genes. Under normal conditions, the physical interaction of PHB and HSFA1s inhibits the transcriptional activity of HSFA1s. Upon HS, the production of miR165/166 is dramatically induced, which in turn represses *PHB* expression. Consequently, the inhibition of PHB on regulation by HSFA1s activity is limited. Our results also show that the miR165/166–*PHB* module can regulate *HSFA1* at the transcriptional level and that PHB represses the expression of *HSFA1*s by binding to their promoter regions. Thus, under nonstress conditions, PHB not only represses the transcription of *HSFA1*s but also inhibits their transcriptional activity. Under HS conditions, the miR165/166-mediated cleavage of *PHB* mRNA is dramatically enhanced, and the negative effect of PHB on the expression of *HSFA1*s and activity of HSFA1s was reduced, leading to increased tolerance to HS.

Transcriptome-wide reprogramming of gene expression is critical for plant responses to HS. HSFA1-mediated transcriptional reprogramming contributes greatly to thermotolerance. Transcriptome profiling analysis of the *hsfa1* quadruple mutant and *PHB* gain-of-function transgenic plants revealed that almost half of the genes regulated by HSFA1 are also controlled by PHB under HS (Fig. 9B). Combined with the evidence that PHB controls the expression of *HSFA1*s and activity of HSFA1s, we hypothesize that PHB can regulate the transcriptional cascade in an HSFA1-dependent manner. Notably, HS-inducible *HSFA2* is also directly regulated by PHB and serves as a common target of HSFA1 and PHB (Fig. 6). We predict that PHB might also orchestrate HS-triggered transcriptional reprogramming in an HSFA1-independent manner, possibly via its direct regulation of *HSFA2* or some other factors.

Our work focused here on the downstream core signaling components underlying thermotolerance and showed that HS-induced accumulation of miR165/166 reduces the transcript levels of miR165/166 target genes (Fig. 1, A to C). How the abundance of miR165/166 is controlled and the underlying mechanism mediating the modulation of miR165/166 under HS is still unknown. Identification of regulatory factors upstream of the miR165/166–*PHB* module will further our understanding of how it regulates HS responses.

HS affects plant growth and development. When confronted with HS, plants utilize different regulators to coordinate their developmental regulatory program and stress responses modulation networks to survive. miR165/166 is an important conserved miRNA and plays a vital role in plant development and HS responses. Like miR165/166, the developmental regulators miR156 and miR160 are also essential HS components (Stief et al. 2014; Lin et al. 2018). These findings suggest that miRNA might mediate environmental regulation of growth and development in plant response to HS. The use of miRNAs to counterbalance the adverse effects of HS on plant growth and development could be a good strategy for plants to respond to HS. Therefore, it is worth identifying more miRNAs involved in HS and deciphering the connection between miRNAs and different HS components. This analysis will provide a deep insight into the mechanism of miRNAs in HS response and eventually facilitate the improvement of crop stress tolerance and yield stability in the future.

Materials and methods

Plant materials and growth conditions

The WT and mutant *Arabidopsis* (*A. thaliana*) plants used in this study were in the Col-0 background. STTM165/166 lines, miR165/166 overexpression lines, *PHBpro:PHBm-FLAG* (a miR165/166 cleavage-resistant version) lines, and *phb phv* double mutant were described previously (Yan et al. 2012). For the generation of *35S:HSFA1b-GFP* transgenic plants, the plasmid was transformed into WT *Arabidopsis* plants by the floral dip method (Clough and Bent 1998). More than 20 independent lines resistance to Basta were isolated and characterized, and T3 transgenic plants were used for analysis. The *Arabidopsis* T-DNA insertion mutants *hsfa1a* (SALK_068042) and *hsfa1d* (SALK_022404) and the *hsfa1b hsfa1e* double mutant (CS2103365) were obtained from the Nottingham Arabidopsis Stock Centre (http://arabidopsis.info/). The triple mutant *hsfa1a hsfa1b hsfa1e* was obtained by crossing the *hsfa1a* single mutant and the *hsfa1b hsfa1e* double mutant. Then, the *hsfa1a hsfa1b hsfa1d hsfa1e* quadruple mutant was generated by crossing the *hsfa1a hsfa1b hsfa1e* triple mutant and the *hsfa1d* single mutant. The *hsfa1a hsfa1b hsfa1d* triple mutant and *hsfa1a hsfa1b hsfa1d hsfa1e* quadruple mutant were identified from the F2 segregating progeny of F1 heterozygous plants. Homozygous plants were isolated by genotyping using the PCR primers listed in Supplemental Table S1. Seeds were surface sterilized and sown on solid culture medium (Murashige–Skoog [MS] salts, 1% [*w*/*v*] sucrose, and 0.6% [*w*/*v*] agar). After 2 d of stratification at 4°C in darkness, seeds were placed into a growth incubator (PERCIVAL) at 22°C in a 16-h light (100 μmol m^{-2} s^{-1}, white LED lamps)/8-h dark photoperiod.

Thermotolerance assays

Thermotolerance assays were performed as described (Guan et al. 2013; Han et al. 2020). Surface-sterilized seeds were sown on MS medium with 1% (*w*/*v*) sucrose and placed in a growth incubator at 22°C in a 16-h light/8-h dark photoperiod. The plates were then transferred to a growth chamber after 7 d for 1 h at 37°C before collecting samples for RT-qPCR analysis.

For basal thermotolerance analysis, 7-d-old seedlings were incubated at 37°C for 24 h and allowed to recover at 22°C for 3 d. For acquired thermotolerance analysis, 7-d-old seedlings were first incubated at 37°C for 1 h and then transferred at 22°C for 2 h. After 2 h at 22°C, seedlings were treated at 44°C for 3.5 h and returned to 22°C.

Three-week-old soil-grown plants were treated at 37°C for 4 d and then allowed to recover at 22°C for 3 d. Photographs

of the damage were taken, and survival rates were measured after 3 d of recovery.

Plasmid construction

To obtain the *35S:HSFA1b-GFP* plasmid, the full-length coding sequence (CDS) of *HSFA1b* was amplified by PCR from WT (Col-0) cDNA and inserted into the *BamHI-SmaI* sites of the pENTR-TOPO vector. The insert was recombined into the pEarlygate 103 vector containing the sequence encoding GFP using the Gateway LR Clonase II Enzyme system (Thermo Fisher).

For in vitro pull-down assays, the full-length CDS of *PHB* was inserted into *SmaI-SalI* sites of the pGEX4T-1 vector to generate *GST-PHB*, and the CDS of *HSFA1a* and *HSFA1b* was individually cloned into the *BamHI-XbaI* and *XbaI-PstI* sites of pMAL-c2x to generate *MBP-HSFA1a* and *MBP-HSFA1b*, respectively.

Two fragments of the *PHB* CDS (from 1 to 390 bp or 391 to 2,556 bp) for yeast 2-hybrid assays were individually cloned into the *NdeI-EcoRI* sites of pGBKT7 (GAL4 DNA-binding domain, Clontech) bait vector, and the full-length CDS of *HSFA1a* or *HSFA1b* was cloned into the *SmaI-BamHI* or *NdeI-EcoRI* sites, respectively, of the pGADT7 (GAL4 activation domain, Clontech) prey vector.

For BiFC assays, the full-length or truncated CDS of *PHB* was inserted into the *SacI-SmaI* sites or *EcoRI-SmaI* sites of the pENTR-TOPO vector respectively and then cloned in-frame with the sequence encoding the N-terminal half of GFP using the pGWB6 to generate the *35S:PHB-nGFP* construct. Similarly, the full-length CDS of *HSFA1a* or *HSFA1b* was first inserted into the *BamHI-SmaI* sites of the pENTR-TOPO vector and then cloned in-frame with the sequence encoding the C-terminal half of GFP using the pGWB5 to obtain the *35S:HSFA1a-cGFP* or *35S:HSFA1b-cGFP* construct, respectively.

To perform the dual-LUC reporter assay, putative promoter sequences (~2.0 kb) of *HSFA1a*, *HSFA1b*, *HSFA2*, *HSP90-1*, and *HSP17.6B* were amplified by PCR from Col-0 genomic DNA and cloned individually into the pGreenII 0800-LUC vector to drive the firefly *LUC* gene, with the *Renilla* luciferase (*REN*) gene controlled by the *35S* promoter. The primer sequences are listed in Supplemental Data Set 1.

RT-qPCR analysis

Total RNA was extracted from 7-d-old seedlings that were ground in liquid nitrogen using TRIzol reagent (Invitrogen) and treated with DNase I (New England Biolabs) to remove genomic DNA contamination. Approximately 4 μg of total RNA was used for first-strand cDNA synthesis with a ReverTra Ace qPCR RT Master Mix (Toyobo). qPCR reactions were performed using a 2× SYBR Green Real-Time PCR Master Mix (Toyobo) on a CFX96 Real-Time PCR system (BioRad). *ACTIN* mRNA was used as an internal control. Three independent biological replicates were conducted, with 3 technical replicates for each biological replicate. The primers used are listed in Supplemental Data Set 1.

Mature miRNA RT-qPCR analysis

Mature miRNA abundance analysis was conducted as previously described (Chen et al. 2005). According to the manufacturer's protocol, total RNA was isolated using an RNeasy mini kit (Qiagen) from 7-d-old seedlings, accompanied by genomic DNA digestion with an RNase-free DNase set (Qiagen). A TaqMan microRNA Reverse Transcription Kit (Invitrogen) was used for miRNA reverse transcription and TaqMan Universal Master Mix II (Thermo Fisher) for qPCR. *Arabidopsis* SnoR101 was used as an internal control. At least 3 independent biological replicates were conducted, with 3 technical replicates for each biological replicate. Primer sequences are listed in Supplemental Data Set 1.

Northern blotting analysis

The northern blotting analysis was conducted as described by Guan et al. (2013). Small RNAs were extracted from 7-d-old WT seedlings with a miRcute miRNA Isolation Kit (TIANGEN) following the manufacturer's protocol. Approximately 30 μg of small RNAs were resolved on 15% polyacrylamide denaturing gels (8 M urea) and transferred onto a Hybond N^+ membrane (Amersham Biosciences, GE Healthcare). The membrane was cross-linked by UV irradiation for 3 min and hybridized with biotin-labeled oligonucleotides at 42°C for 12 h. The membrane signals were detected with a Chemiluminescent Nucleic Acid Detection Module Kit (Thermo Fisher). The U6 probe was used as the control. Three biological replicates were performed, and the sequences of the oligonucleotides used as probes are listed in Supplemental Data Set 1.

RNA-seq analysis

Total RNA was extracted from 7-d-old WT, *PHBpro:PHBm-FLAG* and *hsfa1a hsfa1b hsfa1d hsfa1e* seedlings grown under normal conditions and 7-d-old WT, *PHBpro:PHBm-FLAG* and *hsfa1a hsfa1b hsfa1d hsfa1e* seedlings with heat treatment (37°C for 1 h) using the TRIzol reagent (Invitrogen). The purity and quantification of RNA were evaluated with a NanoDrop 2000 spectrophotometer (Thermo Fisher), while RNA integrity was assessed with an Agilent 2100 Bioanalyzer (Agilent Technologies, Santa Clara). For library construction, a VAHTS Universal V6 RNA-seq Library Prep Kit was used.

Transcriptome sequencing and subsequent analysis were performed by OE Biotech Co., Ltd. (Shanghai, China) using an Illumina Novaseq 6000 platform. After removal of low-quality reads with Q20 <85%, clean reads were mapped to the *Arabidopsis* reference genome (TAIR10.1-NCBI) using HISAT2 (Kim et al. 2015). Principal component analysis (PCA) was conducted to evaluate the biological replication of samples using R (v 3.2.0). Differential expression analysis was conducted using DESeq2 R package (Love et al. 2014). GO enrichment analysis of differentially expressed genes (DEGs) was conducted using clusterprofile (v4.6.0) to look for significantly enriched terms. *P*-values were adjusted using

the Benjamini and Hochberg approach. In each pair-wise comparison, genes with $|log_2$ fold-change$| > 0.6$ and a P-value < 0.05 found by DEseq2 were considered as differentially expressed.

ChIP assays

ChIP assays were conducted as previously described (Guan et al. 2013). Briefly, 7-d-old *PHBpro:PHBm-FLAG*, *35S:HSFA1b-GFP*, *35S:HSFA1b-GFP PHBpro:PHBm-FLAG*, and *35S:HSFA1b-GFP* miR165/166-OE seedlings were used. Approximately 3 g of seedlings was fixed for 20 min with 1% (*w*/*v*) formaldehyde. Glycine (125 mM) was added to terminate cross-linking, and the samples were ground to powder. Chromatin extracts were isolated with 25 mL of isolation buffer and sheared into ∼500-bp fragments with a sonicator (Diagenode) and were then precleared using protein A/G agarose beads (Santa Cruz). DNA precipitated by 5 μL of anti-GFP (Abmart, P30010L) or anti-FLAG (Abmart, M20008L) antibodies was washed for 10 min using 4 different buffers (low salt buffer; high salt buffer; LiCl buffer; and TE buffer) at 4°C and then reverse cross-linked in a 65°C incubator for 12 h. Proteinase K (1 mg/mL) was used to remove proteins at 45°C for 1 h. qPCR was performed with the purified DNA. IgG (Abmart, B30011M) was used as the negative control. Three independent biological replicates were conducted. Primers used in the ChIP-qPCR assays are listed in Supplemental Data Set 1.

EMSAs

EMSAs were conducted essentially as described previously (Li et al. 2014). Recombinant GST-PHB and MBP-HSFA1b were produced in the BL21 strain of *Escherichia coli*. Oligonucleotide probes (∼65 bp) were synthesized with their 3′ end labeled with biotin by Sangon Biotech Co., Ltd. (Shanghai, China). To generate double-stranded probes, sense and antisense oligonucleotide probes were heated for 10 min at 95°C and cooled down to room temperature. EMSA was carried out using a Light Shift Chemiluminescent EMSA Kit (Thermo Fisher). The reaction mixtures were incubated at room temperature for ∼25 min and electrophoresed on 6% native polyacrylamide gels in 0.5× Tris borate EDTA (TBE) at 100 V for 100 min. Then, the DNA was electrophoretically transferred to nylon membranes (GE Healthcare) at 400 mA for 30 min. The resulting membranes were exposed to UV light for ∼5 min to cross-link the transferred free probes and bound probes to the membrane and then washed with buffers. Signals were detected by a Tanon-5500 Chemiluminescent Imaging System (Tanon, China). The relevant oligonucleotide sequences are listed in Supplemental Data Set 1.

Yeast 2-hybrid assays

Yeast 2-hybrid assays were carried out as previously described (Li et al. 2014). The constructs were transformed into the yeast strain AH109 (Clontech). Yeast cells were plated onto selective medium SD/−Leu/−Trp/−His (−LTH). 3-amino-1,2,4-triazole (3-AT) was added to the selection medium to reduce the autoactivation of reporter genes. The relevant primer sequences are listed in Supplemental Data Set 1.

In vitro pull-down assays

Pull-down analysis was performed according to Friedrich et al. (2021). Recombinant GST and MBP fusion proteins were produced in the BL21 strain of *E. coli* and then were purified using Mag-Beads GST (Sangon, China) or Amylose Resin (New England Biolabs). The purified proteins were immunoblotted with anti-GST (GenScript, 1:2,000) or anti-MBP (New England Biolabs, 1:5,000) antibodies. The relevant primer sequences are listed in Supplemental Data Set 1.

BiFC assays

BiFC assays were conducted as previously described (Li et al. 2014). The constructs were transformed into *Agrobacterium* (*Agrobacterium tumefaciens*) strain GV3101. Constructs harboring sequences encoding the C- or N-terminal halves of GFP were co-infiltrated in young leaves of *N. benthamiana*. After 48 h, infiltrated leaves were harvested to detect GFP fluorescence signals. Additionally, plasmids were also co-transfected into *Arabidopsis* protoplasts using the polyethylene glycol-mediated (PEG-mediated) transient transformation method (Yoo et al. 2007), and GFP fluorescence signals were observed after 12 h of incubation. GFP fluorescence signals were detected using a microscope (Zeiss Imager A2) with the GFP filter (excitation band EX 470/40 nm, emission band EM530/40 nm). The *Arabidopsis* protoplast assay was performed as previously described (Marion et al. 2008). At least 3 independent experiments were conducted using different batches of plants. More than 6 plants were infiltrated, and over 500 protoplasts were examined for each independent biological replicate. The relevant primer sequences are listed in Supplemental Data Set 1.

Dual-LUC assays

Dual-LUC assays and transient expression assays were carried out as previously described by Hu et al. (2019). In brief, the vectors, *35S:GFP*, *35S:PHB-GFP*, and *35S:HSFA1b-GFP*, were used as effectors. The vectors, *HSFA1apro:LUC*, *HSFA1bpro:LUC*, *HSFA2pro:LUC*, *HSP90-1pro:LUC*, and *HSP17.6Bpro:LUC*, were used as reporters. Effector and reporter constructs were co-infiltrated as appropriate pairs into *N. benthamiana* leaves via *Agrobacterium*, and leaves were collected 48 h after infiltration. The LUC and REN activity values were determined with a Dual-LUC Reporter Assay System (Promega) on a Synergy NEO2 luminometer (BioTek), and then LUC activity was normalized to REN. The relevant prime sequences are listed in Supplemental Data Set 1.

Co-IP assays

Co-immunoprecipitation assays were performed as previously described (Friedrich et al. 2021). Briefly, the *35S:PHB-FLAG*, *35S:HSFA1a-GFP*, and *35S:HSFA1b-GFP* plasmids were

transformed into *Agrobacterium* strain GV3101 and co-infiltrated into young *N. benthamiana* leaves. After 48 h, total proteins were extracted from leaves using protein extraction kit (CWBIO, CW0885) and incubated overnight with anti-FLAG antibody (Abmart, M20008L, 1:5,000). The immunocomplexes were then collected by protein A/G agarose beads (Santa Cruz) and washed with immunoprecipitation buffer. The eluted proteins were subsequently detected by immunoblotting using an anti-GFP antibody (Abmart, P30010L, 1:5,000).

Statistical analysis

Statistical analyses were performed as described in each figure legend. Statistical data are provided in Supplemental Data Set 2.

Accession numbers

Raw RNA-seq reads were deposited at the National Center for Biotechnology Information (NCBI) under the accession number PRJNA911441. The sequence data for genes in this article can be found in The Arabidopsis Information Resource under the following accessions numbers: *PHB* (At2g34710), *PHV* (At1g30490), *HSFA1a* (At4g17750), *HSFA1b* (At5g16820), *HSFA1d* (At1g32330), *HSFA1e* (At3g02990), *HSFA2* (At2g26150), *HSP90-1* (At5g52640), *HSP17.6B* (At2g29500), *HSP101* (At1g74310), *HSP17.4B* (At1g54050), *HSP17.4* (At3g46230), and *HSP17.6C* (At1g53540).

Acknowledgments

We are grateful to Drs. Xianzhong Feng and Zhong Zhao for their assistance or helpful discussions. We also thank Drs. Zhongnan Yang and Jirong Huang for generously providing the pGreenII-0800 vector and the BiFC vectors.

Author contributions

J.Y. designed the research. J.L., Y.C., J.Z., and C.Z. conducted the research. J.L., Y.C., J.Z., C.Z., G.T., and J.Y. analyzed the data. J.L., G.T., and J.Y. wrote and edited the manuscript.

Supplemental data

The following materials are available in the online version of this article.

The following materials are available in the online version of this article.

Supplemental Figure S1. Thermotolerance analysis of 7-d-old WT, miR165/166-OE and *phb phv* seedlings.

Supplemental Figure S2. Thermotolerance phenotype and survival rate of soil-grown WT and miR165/166-OE.

Supplemental Figure S3. Thermotolerance phenotype and survival rate of soil-grown WT and the *phb phv* double mutant.

Supplemental Figure S4. Thermotolerance analysis of 7-d-old WT, STTM165/166 and *PHBpro:PHBm-FLAG* seedlings.

Supplemental Figure S5. Thermotolerance phenotype and survival rate of soil-grown WT and STTM165/166.

Supplemental Figure S6. Thermotolerance phenotype and survival rate of soil-grown WT and *PHBpro:PHBm-FLAG*.

Supplemental Figure S7. EMSA showing the direct binding of PHB to the promoter regions of *HSFA1a* or *HSFA1b*.

Supplemental Figure S8. Transient dual-LUC reporter assay in *N. benthamiana* leaves showing that PHB suppresses the promoter activity of *HSFA1a* and *HSFA1b*, whereas $PHB^{131-852}$ lacking the DNA-binding domain does not.

Supplemental Figure S9. ChIP assay showing that PHB is enriched on the promoter region of *HSFA1d* or *HSFA1e*.

Supplemental Figure S10. Expression analysis of *HSP* genes in WT, *PHBpro:PHBm-FLAG*, STTM165/166, and miR165/166-OE grown at 22°C or exposed to 37°C for 1 h.

Supplemental Figure S11. EMSA showing the direct binding of PHB to promoter regions of *HSFA2*.

Supplemental Figure S12. Transient dual-LUC reporter assay in *N. benthamiana* leaves showing that PHB suppresses the promoter activity of *HSFA2*, whereas $PHB^{131-852}$ lacking of DNA-binding domain does not.

Supplemental Figure S13. EMSA assay showing that PHB antagonizes HSFA1b to bind to the promoters of *HSP90-1* and *HSP17.6B*.

Supplemental Figure S14. Analysis of *35S:HSFA1b-GFP*, *35S:HSFA1b-GFP PHBpro:PHBm-FLAG*, and *35S:HSFA1b-GFP* miR165/166-OE transgenic plants.

Supplemental Figure S15. The enhanced thermotolerance phenotype of miR165/166-OE is suppressed when they in the *hsfa1a hsfa1b hsfa1d* mutant background.

Supplemental Data Set 1. Oligonucleotides used in this study.

Supplemental Data Set 2. Summary of statistical analyses.

Funding

This work was supported by grants from Science and Technology Commission of Shanghai Municipality, China (No.18PJ1402800, 20ZR1417900, and 22N11900400).

Conflict of interest statement. The authors declare no competing interests.

References

Baker CC, Sieber P, Wellmer F, Meyerowitz EM. The early extra petals1 mutant uncovers a role for microRNA miR164c in regulating petal number in *Arabidopsis*. Curr Biol. 2005:**15**(4):303–315. https://doi.org/10.1016/j.cub.2005.02.017

Baniwal SK, Bharti K, Chan KY, Fauth M, Ganguli A, Kotak S, Mishra SK, Nover L, Port M, Scharf K-D, et al. Heat stress response in plants: a complex game with chaperones and more than twenty heat stress transcription factors. J Biosci. 2004:**29**(4):471–487. https://doi.org/10.1007/BF02712120

Busch W, Wunderlich M, Schöffl F. Identification of novel heat shock factor-dependent genes and biochemical pathways in *Arabidopsis*

thaliana. Plant J. 2005:**41**(1):1–14. https://doi.org/10.1111/j.1365-313X.2004.02272.x

Carlsbecker A, Lee JY, Roberts CJ, Dettmer J, Lehesranta S, Zhou J, Lindgren O, Moreno-Risueno MA, Vatén A, Thitamadee S, et al. Cell signalling by microRNA165/6 directs gene dose-dependent root cell fate. Nature 2010:**465**(7296):316–321. https://doi.org/10.1038/nature08977

Charng YY, Liu HC, Liu NY, Chi WT, Wang CN, Chang SH, Wang TT. A heat-inducible transcription factor, HsfA2, is required for extension of acquired thermotolerance in *Arabidopsis*. Plant Physiol. 2007:**143**(1):251–262. https://doi.org/10.1104/pp.106.091322

Chen C, Ridzon DA, Broomer AJ, Zhou Z, Lee DH, Nguyen JT, Barbisin M, Xu NL, Mahuvakar VR, Andersen MR, et al. Real-time quantification of microRNA by stem-loop RT-PCR. Nucleic Acids Res. 2005:**33**(20):e179. https://doi.org/10.1093/nar/gni178

Clough SJ, Bent AF. Floral dip: a simplified method for *Agrobacterium*-mediated transformation of *Arabidopsis thaliana*. Plant J. 1998:**16**(6):735–743. https://doi.org/10.1046/j.1365-313x.1998.00343.x

Czarnecka-Verner E, Pan S, Salem T, Gurley WB. Plant class B HSFs inhibit transcription and exhibit affinity for TFIIB and TBP. Plant Mol Biol. 2004:**56**(1):57–75. https://doi.org/10.1007/s11103-004-2307-3

Fang X, Zhao G, Zhang S, Li Y, Gu H, Li Y, Zhao Q, Qi Y. Chloroplast-to-nucleus signaling regulates microRNA biogenesis in *Arabidopsis*. Dev Cell. 2019:**48**(3):371–382.e4. https://doi.org/10.1016/j.devcel.2018.11.046

Friedrich T, Oberkofler V, Trindade I, Altmann S, Brzezinka K, Lämke J, Gorka M, Kappel C, Sokolowska E, Skirycz A, et al. Heteromeric HSFA2/HSFA3 complexes drive transcriptional memory after heat stress in Arabidopsis. *Nat Commun*. 2021:(1):3426–3441. http://doi.org/10.1038/s41467-021-23786-6

Fujii H, Chinnusamy V, Rodrigues A, Rubio S, Antoni R, Park SY, Cutler SR, Sheen J, Rodriguez PL, Zhu JK. In vitro reconstitution of an abscisic acid signalling pathway. Nature 2009:**462**(7273):660–664. https://doi.org/10.1038/nature08599

Fujii H, Chiou TJ, Lin SI, Aung K, Zhu JK. A miRNA involved in phosphate-starvation response in *Arabidopsis*. Curr Biol. 2005:**15**-(22):2038–2043. https://doi.org/10.1016/j.cub.2005.10.016

Guan Q, Lu X, Zeng H, Zhang Y, Zhu J. Heat stress induction of miR398 triggers a regulatory loop that is critical for thermotolerance in *Arabidopsis*. Plant J. 2013:**74**(5):840–851. https://doi.org/10.1111/tpj.12169

Han SH, Park YJ, Park CM. HOS1 activates DNA repair system to enhance plant thermotolerance. Nat Plants 2020:**6**(12):1439–1446. http://doi.org/10.1038/s41477-020-00809-6

Hu Y, Han X, Yang M, Zhang M, Pan J, Yu D. The transcription factor INDUCER OF CBF EXPRESSION1 interacts with ABSCISIC ACID INSENSITIVE5 and DELLA proteins to fine-tune abscisic acid signaling during seed germination in *Arabidopsis*. Plant Cell 2019:**31**(7):1520–1538. https://doi.org/10.1105/tpc.18.00825

Ikeda M, Mitsuda N, Ohme-Takagi M. *Arabidopsis* HsfB1 and HsfB2b act as repressors of the expression of heat-inducible HSFs but positively regulate the acquired thermotolerance. Plant Physiol. 2011:**157**(3):1243–1254. https://doi.org/10.1104/pp.111.179036

Ikeda M, Ohme-Takagi M. A novel group of transcriptional repressors in *Arabidopsis*. Plant Cell Physiol. 2009:**50**(5):970–975. https://doi.org/10.1093/pcp/pcp048

Jia X, Ding N, Fan W, Yan J, Gu Y, Tang X, Li R, Tang G. Functional plasticity of miR165/166 in plant development revealed by small tandem target mimic. Plant Sci. 2015:**233**:11–21. https://doi.org/10.1016/j.plantsci.2014.12.020

Jones-Rhoades MW, Bartel DP. Computational identification of plant microRNAs and their targets, including a stress-induced miRNA. Mol Cell. 2004:**14**(6):787–799. https://doi.org/10.1016/j.molcel.2004.05.027

Jones-Rhoades MW, Bartel DP, Bartel B. MicroRNAS and their regulatory roles in plants. Annu Rev Plant Biol. 2006:**57**(1):19–53. https://doi.org/10.1146/annurev.arplant.57.032905.105218

Khraiwesh B, Zhu JK, Zhu J. Role of miRNAs and siRNAs in biotic and abiotic stress responses of plants. Biochim Biophys Acta. 2012:**1819**(2):137–148. https://doi.org/10.1016/j.bbagrm.2011.05.001

Kim D, Langmead B, Salzberg SL. HISAT: a fast spliced aligner with low memory requirements. Nat Methods. 2015:**12**(4):357–360. https://doi.org/10.1038/nmeth.3317

Kumar M, Busch W, Birke H, Kemmerling B, Nurnberger T, Schoffl F. Heat shock factors HsfB1 and HsfB2b are involved in the regulation of Pdf1.2 expression and pathogen resistance in *Arabidopsis*. Mol Plant. 2009:**2**(1):152–165. https://doi.org/10.1093/mp/ssn095

Lauter N, Kampani A, Carlson S, Goebel M, Moose S. MicroRNA172 down-regulates glossy15 to promote vegetative phase change in maize. Proc Natl Acad Sci USA. 2005:**102**(26):9412–9417. https://doi.org/10.1073/pnas.0503927102

Li Y, Li X, Yang J, He Y. Natural antisense transcripts of MIR398 genes suppress microR398 processing and attenuate plant thermotolerance. Nat Commun. 2020:**11**(1):5351. https://doi.org/10.1038/s41467-020-19186-x

Li S, Liu J, Liu Z, Li X, Wu F, He Y. HEAT-INDUCED TAS1 TARGET1 mediates thermotolerance via HEAT STRESS TRANSCRIPTION FACTOR A1a-directed pathways in *Arabidopsis*. Plant Cell 2014:**26**(4):1764–1780. https://doi.org/10.1105/tpc.114.124883

Lin JS, Kuo CC, Yang IC, Tsai WA, Shen YH, Lin CC, Liang YC, Li YC, Kuo YW, King YC, et al. MicroRNA160 modulates plant development and heat shock protein gene expression to mediate heat tolerance in *Arabidopsis*. Front Plant Sci. 2018:**9**:68. https://doi.org/10.3389/fpls.2018.00068

Love MI, Huber W, Anders S. Moderated estimation of fold change and dispersion for RNA-seq data with DESeq2. Genome Biol. 2014:**15**(12):550. https://doi.org/10.1186/s13059-014-0550-8

Lucas WJ, Groover A, Lichtenberger R, Furuta K, Yadav SR, Helariutta Y, He XQ, Fukuda H, Kang J, Brady SM, et al. The plant vascular system: evolution, development and functions. J Integr Plant Biol. 2013:**55**(4):294–388. https://doi.org/10.1111/jipb.12041

Marion J, Bach L, Bellec Y, Meyer C, Gissot L, Faure JD. Systematic analysis of protein subcellular localization and interaction using high-throughput transient transformation of Arabidopsis seedlings. *Plant J*. 2008:**56**(1):169–179. http://doi.org/10.1111/j.1365-313X.2008.03596.x

Mcconnell JR, Emery JF, Eshed Y, Bao N, Bowman J, Barton MK. Role of *PHABULOSA* and *PHAVOLUTA* in determining radial patterning in shoots. Nature 2001:**411**(6838):709–713. https://doi.org/10.1038/35079635

Nover L, Bharti K, Döring P, Mishra SK, Ganguli A, Scharf KD. *Arabidopsis* and the heat stress transcription factor world: how many heat stress transcription factors do we need? Cell Stress Chaperones 2001:**6**(3):177–189. https://doi.org/10.1379/1466-1268(2001)006<0177:AATHST>2.0.CO;2

Ohama N, Kusakabe K, Mizoi J, Zhao H, Kidokoro S, Koizumi S, Takahashi F, Ishida T, Yanagisawa S, Shinozaki K, et al. The transcriptional cascade in the heat stress response of *Arabidopsis* is strictly regulated at the level of transcription factor expression. Plant Cell 2016:**28**(1):181–201. https://doi.org/10.1105/tpc.15.00435

Ohama N, Sato H, Shinozaki K, Yamaguchi-Shinozaki K. Transcriptional regulation network of plant heat stress response. Trends in Plant Sci. 2017:**22**(1):53–65. https://doi.org/10.1016/j.tplants.2016.08.015

Otsuga D, De Guzman B, Prigge MJ, Drews GN, Clark SE. *REVOLUTA* regulates meristem initiation at lateral positions. Plant J. 2001:**25**(2):223–236. https://doi.org/10.1046/j.1365-313x.2001.00959.x

Prigge MJ, Otsuga D, Alonso JM, Ecker JR, Drews GN, Clark SE. Class III homeodomain-leucine zipper gene family members have overlapping, antagonistic, and distinct roles in *Arabidopsis* development. Plant Cell 2005:**17**(1):61–76. https://doi.org/10.1105/tpc.104.026161

Reyes JL, Chua NH. ABA induction of miR159 controls transcript levels of two MYB factors during *Arabidopsis* seed germination. Plant J. 2007:**49**(4):592–606. https://doi.org/10.1111/j.1365-313X.2006.02980.x

Rogers K, Chen X. Biogenesis, turnover, and mode of action of plant microRNAs. Plant Cell 2013:**25**(7):2383–2399. https://doi.org/10.1105/tpc.113.113159

Sessa G, Carabelli M, Possenti M, Morelli G, Ruberti I. Multiple links between HD-Zip proteins and hormone networks. Int J Mol Sci. 2018:**19**(12):4047. -. https://doi.org/10.3390/ijms19124047

Smith ZR, Long JA. Control of *Arabidopsis* apical-basal embryo polarity by antagonistic transcription factors. Nature 2010:**464**(7287):423–426. https://doi.org/10.1038/nature08843

Stief A, Altmann S, Hoffmann K, Pant BD, Scheible WR, Baurle I. *Arabidopsis* miR156 regulates tolerance to recurring environmental stress through SPL transcription factors. Plant Cell 2014:**26**(4):1792–1807. https://doi.org/10.1105/tpc.114.123851

Sunkar R, Zhu JK. Novel and stress-regulated microRNAs and other small RNAs from *Arabidopsis*. Plant Cell 2004:**16**(8):2001–2019. https://doi.org/10.1105/tpc.104.022830

Trent JD. A review of acquired thermotolerance, heat-shock proteins, and molecular chaperones in archaea. FEMS Microbiol Rev. 1996:**18**(2–3):249–258. https://doi.org/10.1111/j.1574-6976.1996.tb00241.x

Vierling E. The roles of heat shock proteins in plants. Annu Rev Plant Physiol Plant Mol Biol. 1991:**42**(1):579–620. https://doi.org/10.1146/annurev.pp.42.060191.003051

Yan J, Gu Y, Jia X, Kang W, Pan S, Tang X, Chen X, Tang G. Effective small RNA destruction by the expression of a short tandem target mimic in *Arabidopsis*. Plant Cell 2012:**24**(2):415–427. https://doi.org/10.1105/tpc.111.094144

Yan J, Zhao C, Zhou J, Yang Y, Wang P, Zhu X, Tang G, Bressan RA, Zhu JK. The miR165/166 mediated regulatory module plays critical roles in ABA homeostasis and response in *Arabidopsis thaliana*. PLoS Genet. 2016:**12**(11):e1006416. https://doi.org/10.1371/journal.pgen.1006416

Yoo SD, Cho YH, Sheen J. *Arabidopsis* mesophyll protoplasts: a versatile cell system for transient gene expression analysis. Nat Protoc. 2007:**2**(7):1565–1572. https://doi.org/10.1038/nprot.2007.199

Yoshida T, Ohama N, Nakajima J, Kidokoro S, Mizoi J, Nakashima K, Maruyama K, Kim J, Seki M, Todaka D, et al. *Arabidopsis* HsfA1 transcription factors function as the main positive regulators in heat shock-responsive gene expression. Mol Genet Genomics. 2011:**286**(5–6):321–332. https://doi.org/10.1007/s00438-011-0647-7

Zhang S, Dou Y, Li S, Ren G, Chevalier D, Zhang C, Yu B. DAWDLE interacts with DICER-LIKE proteins to mediate small RNA biogenesis. Plant Physiol. 2018:**177**(3):1142–1151. https://doi.org/10.1104/pp.18.00354

Zhou GK, Kubo M, Zhong R, Demura T, Ye ZH. Overexpression of miR165 affects apical meristem formation, organ polarity establishment and vascular development in *Arabidopsis*. Plant Cell Physiol. 2007:**48**(3):391–404. https://doi.org/10.1093/pcp/pcm008